ADVANCED ELECTRONIC MATERIALS

# Supporting Information

for *Adv. Electron. Mater.*, DOI: 10.1002/aelm.201600351

# Monitoring of Energy Conservation and Losses in Molecular Junctions through Characterization of Light Emission

*Oleksii Ivashenko, Adam Johan Bergren,* and Richard L. McCreery**

**Monitoring of Energy Conservation and Losses in Molecular Junctions through Characterization of Light Emission**

*Oleksii Ivashenko, Adam Johan Bergren, and Richard L. McCreery*[*]

Dr. O. Ivashenko, Prof. R. L. McCreery
University of Alberta, 11421 Saskatchewan Dr. Edmonton, AB T6G 2M9, Canada
E-mail: McCreery@ualberta.ca

Dr. A. J. Bergren, Prof. R. L. McCreery
National Institute for Nanotechnology, 11421 Saskatchewan Dr. Edmonton, AB T6G 2M9, Canada
E-mail: Adam.Bergren@nrc.ca

Keywords: hot carriers, charge transport, molecular electronics, light emission

**Abstract:** Emission of visible light from large area molecular junctions provides a direct measure of the energy of carriers when they encounter a conducting contact and stimulate photon emission. For carbon/molecule/carbon molecular junctions containing aromatic molecular layers with thicknesses less than 5 nm, transport is elastic, and the maximum emitted photon energy (i.e. "cut off" energy, $h\nu_{co}$) is equal to $eV_{app}$, where $V_{app}$ is the bias across the molecular junction. $h\nu_{co}$ increases monotonically with $V_{app}$, is symmetric with polarity, but is weakly dependent on the nature of the contact material. Light emission from molecular junctions containing oligomeric films of anthraquinone (AQ), nitroazobenzene (NAB), naphthalene diimide (NDI) and bis-thienyl benzene (BTB) with thicknesses of 4.5 to 59 nm was observed as a function of bias. For layers thicker than 5-7 nm $h\nu_{co} < eV_{app}$, indicating loss of energy and therefore inelastic transport. The energy loss depends strongly on molecular structure and is linear with molecular layer thickness. As molecular layer thickness exceeds 5-7 nm, the results provide strong evidence for a transition from elastic to inelastic transport and for stepwise, activationless transport up to 65 nm molecular layer thicknesses. Such information should prove valuable for determining transport mechanisms and ultimately designing molecular junctions with desirable electronic properties.

## 1. Introduction

Molecular electronics is an area of study that seeks to understand devices that use molecules as circuit components,[1] and was recently realized commercially in audio processing.[2] Many paradigms are used in molecular electronics, including methods for making electrical contact to single molecules as well as large area molecular junctions that contain many billions of molecules oriented between two conductive contacts. In general, the distance of charge transport in molecular devices is comparable to the length of small molecules (~10 nm or less), but there have been cases in which thicker films are used in order to gain insights into nanoscale charge transport[3], Several groups have shown that the electronic characteristics of molecular devices are consistent with quantum mechanical tunneling[4] for molecular layer thicknesses less than ~6 nm. A transition from tunneling to other transport mechanisms above 6 nm has been noted, and proposals for this "beyond tunneling" regime include activated hopping[5] and field ionization.[3b] Additional mechanisms have also been proposed as a function of variables other than thickness, including voltage, electric field, and temperature.[6]

Hot carrier devices are emerging as a platform for making functional electronic devices with possible applications in optics, energy capture, chemistry, and plasmonics.[6a] This platform relies on carriers in a non-equilibrium state (i.e., with excess energy compared to electrons in bulk) to stimulate physical or chemical phenomenon such as chemical reactions,[7] local heating,[6a] and light emission.[8] In the last case, hot carriers generated electronically can interact with plasmons in metal structures, which can then decay by emission of photons. In past work, light emission from inorganic metal-oxide-metal (M-O-M) tunnel junctions has been correlated with plasmonic excitation and decay.[9] The hot carriers were generated by quantum mechanical tunneling across thin (~3 nm) oxide barriers, which resulted in low efficiency broadband light emission that could be correlated with the applied voltage and the plasmonic nature of the top contact (i.e., its identity and roughness). It is important to note that the process can be reversed, so that incident light may generate hot carriers in some devices. In these

cases, a photocurrent produced by internal photoemission[10] can be used to characterize transport barriers and other important device features (such as when the molecule absorbs light).[11]

Following the initial observation of light emission from M-O-M structures,[12] light emission originating from metal-molecule-STM tip structures has also been reported. While bare metal STM tips over conductors were shown to emit light due to localized surface plasmons excited by inelastic tunneling electrons [13], molecules adsorbed onto the surface enhanced the effect.[14] In these cases, two processes were proposed: 1) decay of localized surface plasmons excited by inelastic tunneling; and 2) fluorescence mediated by injection of hot carriers into molecular LUMOs.[15] Since close proximity of metallic surfaces is known to quench radiative transitions, the observation of light emission from molecular films involved oxide or long molecular spacers to decouple molecules from the metal.[15b, 16] Finally, luminescence from a complete single molecule junction consisting of a naphthalenediimide chromophore bridging two metallic carbon nanotubes was reported,[17] for which a mechanism involving molecular orbitals similar to that proposed for light emission from organic light emitting diodes (OLEDs) was invoked.

We have reported light emitting "all carbon" molecular junctions[3a] with the characteristics of the emitted light depending strongly on both molecular structure and molecular layer thickness. For thin molecular layers, the highest emitted photon energy, or "cut-off" energy, $h\nu_{co}$, was determined by the applied bias ($V_{app}$), according to the relation $h\nu_{co} = eV_{app}$, where $h$ is Planck's constant and $e$ is the charge on an electron. A recent report by Nijhuis et al., [18] describes light emission by large area molecular junctions based on Ag/thiol self-assembled monolayers, for which emitted light originates in "hot spots" attributed to nonuniform contacts between the metallic conductors and the molecular layer. The polarization of the emitted light and its spectral distribution varied with applied bias and polarity. Both of these recent results establish that electrons transported across a molecular junction can couple to surface plasmons in the contacts which can then emit light. In addition, we observed a linear

decrease of the emitted photon energy with increasing molecular layer thickness, and attributed the change to losses in carrier energy during transport in thicker films. The current report expands the initial paper in several aspects and addresses the following additional points: 1. light emission from a wider range of molecular structures; 2. the effect of contact materials and the origin of photoemission; 3. demonstration of activationless charge transfer through 65 nm; and 4. deductions about charge transfer mechanisms over distances of 5-65 nm. Note that light emission from molecular junctions [3a, 18] differs fundamentally from that in widely-studied organic light emitting diodes (OLEDs), since the mechanism involves hot carriers coupling to plasmons rather than the electron/hole recombination reactions required in OLEDs.

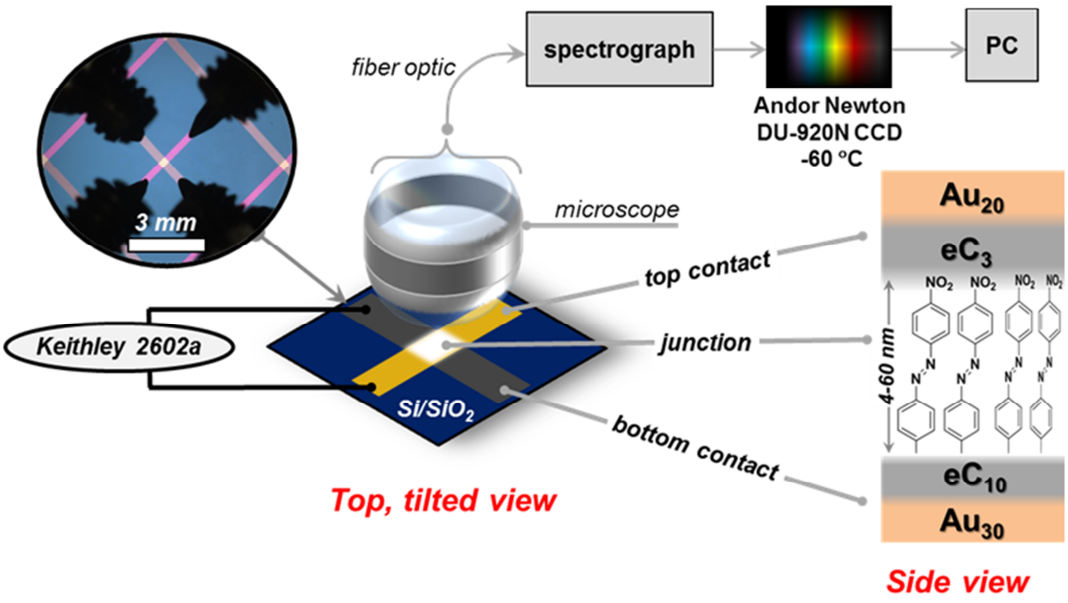


**Figure 1.** Experimental schematic for monitoring light emission from molecular junctions consisting of 4-60 nm thick layers of organic molecules (as shown for NAB) between conducting contacts. Upper left photo is a working device and probes viewed through the collection microscope objective. Many details can be found in the main text, as well as in a previous report.[3a] Subscripts on the schematic of lower right indicate layer thickness in nm, and junction area was 0.00068 $cm^2$.

## 2. Results

The molecular junction (MJ) design has been described in detail previously and consists of diazonium-derived organic oligomers between conducting carbon contacts. [3a, 11a, 19] Additional details relevant to light emission are provided in the Experimental section below and in Supporting Information (SI), and in all cases the MJ was based on electron-beam deposited carbon (eC) contacts, with the structure $Au_{30}/eC_{10}/Mol_x/eC_3/Au_{20}$ noted in **Figure 1**, where the subscripts designate the layer thicknesses in nm. Current density vs bias voltage (*JV*) curves for a range of thicknesses for MJs containing oligomers of nitroazobenzene (NAB), bis-thienyl benzene (BTB), 2-Anthraquinone (AQ), and a naphthalene di-imide derivative (NDI) are shown in **Figure 2**, all at room temperature.

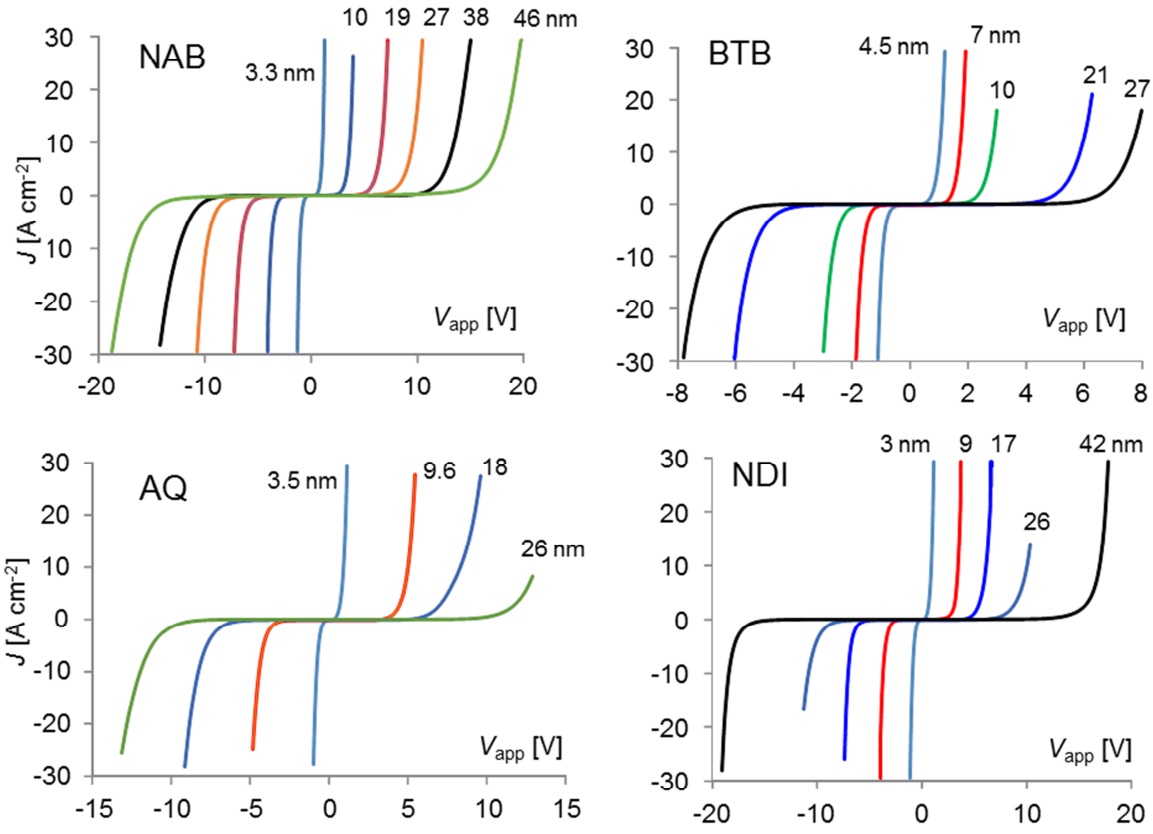


**Figure 2.** *JV* curves for $Au_{30}/eC_{10}/Mol_x/eC_3/Au_{20}$ MJs containing the indicated molecules, with the numbers on each curve denoting molecular layer thickness in nm. In all cases, $V_{app}$ was initiated at 0 volts with a Keithley 2602 source-measurement unit, and required < 1 second for data acquisition. The polarity of $V_{app}$ is the bottom Au contact relative to the top, with subsequent light emission observed from the top (20 nm) Au contact. Additional *JV* curves are provided in Supporting Information figure S1.

The *JV* behavior for thick molecular junctions (*d>30*, in nm) is presented for the first time, while curves for thinner junctions are in agreement with those of thin molecular layers reported previously,[4c, 11a, 19c, 20] but in all cases herein the curves shown are for the same devices as those used for light emission. The *JV* response for eC/BTB/eC devices is very similar to that reported previously with a pyrolyzed carbon substrate and eC top contact, with BTB layers from 4.5 to 22 nm thick.[3b] In all cases, *J* decreases rapidly with increasing thickness, and the *JV* curves are approximately symmetric with respect to bias polarity, with positive polarity at the bottom electrode yielding slightly higher current. Note that for all cases it is possible to achieve high current density (> 20 A/cm$^2$), even for thick films. **Figure 3** compares the *JV* responses for the four molecules with thicknesses of 9-10 and 26-27 nm, and a similar plot for *d* = 7-8 nm was presented in our initial communication.[3a]

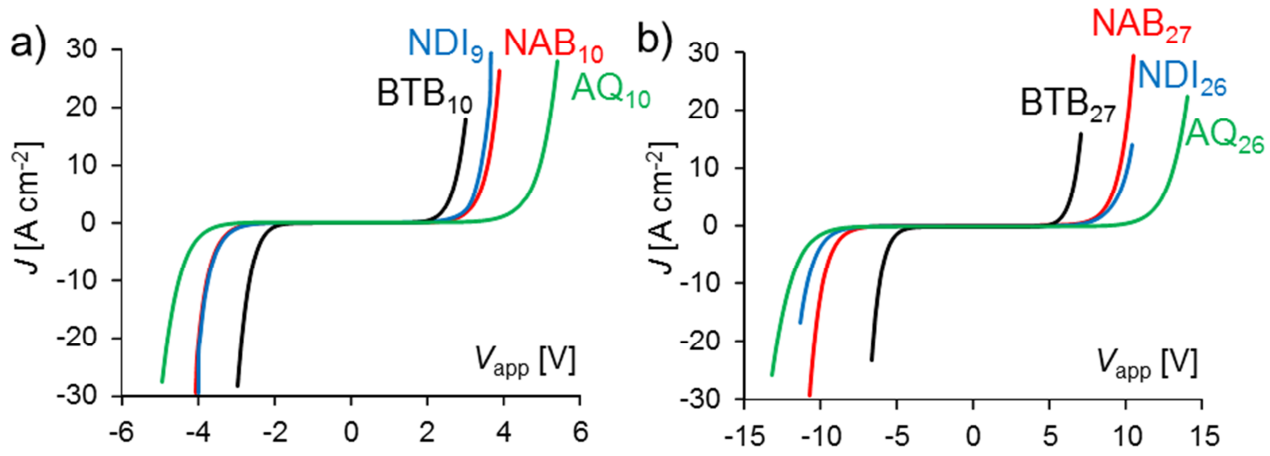


**Figure 3.** Comparison of *JV* responses for four molecules with similar thickness of a) 9-10 nm and b) 26-27 nm. Conditions same as those in Figure 2.

**Figure 4**a shows light emission spectra for an NAB junction with *d* = 10 nm, plotted as CCD response per second for a series of bias values from -4.3 to -5.5 V (bottom contact relative to top), viewed from the top of the junction (i.e., the $eC_3/Au_{20}$ contact). A low initial constant bias was applied for 30 seconds of light collection, then the bias was made progressively more negative and collection repeated. Both the emitted light intensity (panel 4a) and the junction current (Figure 2) increase rapidly

with more negative $V_{app}$. As noted previously,[3a] the maximum emitted photon energy increases with bias for all molecules and junctions examined. Emission from an Al/AlOx/eC/Au junction is included in Figure 4a to demonstrate that the junction structure is capable of generating and emitting photons with energies at least up to 3.3 eV. Figure 4b shows the results of 4a divided by the junction current, in order to more readily compare devices of different type. The most important feature of the spectra in Figure 4a/b is the high-energy cut-off ($h\nu_{co}$), as determined by the intercept of the emission curve with the abscissa. The value of $h\nu_{co}$ indicates the energy of the most energetic photon emitted by the MJ, and is more evident in 4c, which shows the same emission curves on a logarithmic ordinate.

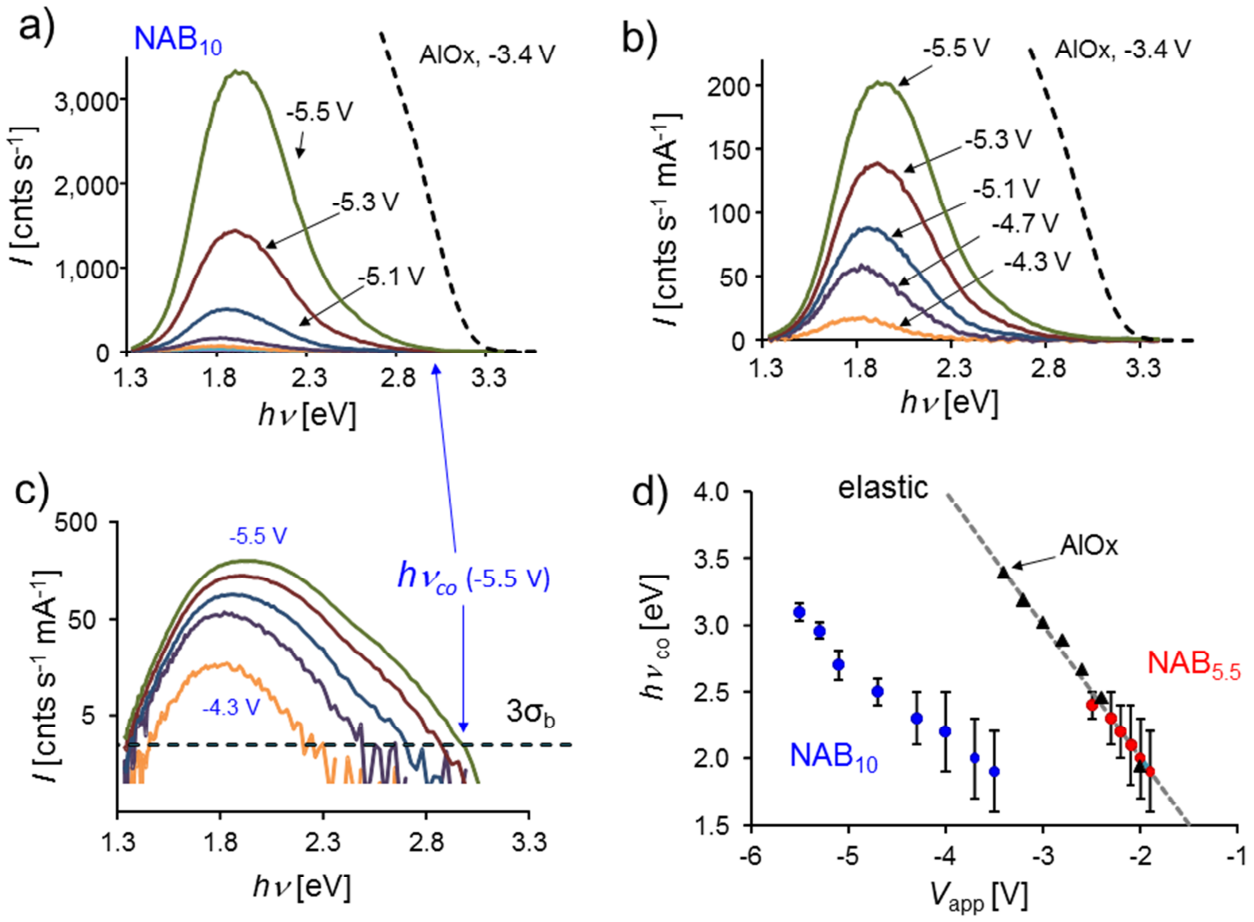


**Figure 4.** Emission spectra from $NAB_{10}$ MJs with progressively negative $V_{app}$, plotted on a linear intensity scale (a), on a scale normalized to junction current (b), and on a logarithmic scale (c). (d) Corresponding $h\nu_{co}$ for $NAB_{10}$, AlOx, and $NAB_{5.5}$ MJs as a function of $V_{app}$. The "elastic" line in d) corresponds to $h\nu_{co} = eV_{app}$. Error bars in (d) were determined as described in SI section 6. The dark signal from the CCD was subtracted from all spectra, and the CCD gain was approximately 1 cnt/photon.

The horizontal dashed line in 4c is a typical detection limit for photon emission, equal to three times the standard deviation of the background (or "dark") response, which was acquired before each emission spectrum. The intercept of the emission curve (or its extrapolated linear portion) on the high energy side with the $3\sigma_b$ line is then taken as $h\nu_{co}$. The monotonic progression of $h\nu_{co}$ with increasing bias apparent in 4c is plotted in Figure 4d, for identical MJs with different NAB layer thicknesses of 10 and 5.5 nm. The dashed line indicates the ideal elastic response, in which the maximum photon energy equals the voltage bias across the MJ, with a slope of -1.0, and was observed for both AlOx and thin NAB layers. The offset and difference in slope for the $NAB_{10}$ MJ compared to $NAB_{5.5}$ shows that $h\nu_{co}$ is lower than $eV_{app}$ for the thicker film. Low energy photons emitted by thin junctions at low bias were more difficult to detect due to the weaker CCD response, and the error in $h\nu_{co}$ increased from < 5% for $h\nu_{co}$ > 2.0 eV to 15% for $h\nu_{co}$ < 2.0 eV (as discussed in SI section 6). Figure S2 shows emission spectra for Al/AlOx/eC/Au reference devices which are qualitatively similar to those of figure 4a, without a molecule or carbon layer present, indicating that light emission occurs for both oxide and molecular tunnel barriers.

The origin of the light emitted by carbon-based MJs was probed initially by considering the symmetry of the *JV* response and light emission as well as the effect of the top contact composition. For all the devices studied, the *JV* curves are essentially symmetric with respect to bias polarity. We have noted this previously for carbon/molecule/Cu [4c] and "all carbon" molecular junctions [3b, 20], and an example from the current devices is shown in figure S3 for AlOx, BTB, and NAB[3a]. Figure 5a shows the emission spectra for an $NAB_8$ MJ biased with opposite polarities but viewed from the same "top contact", as shown in Figure 1, i.e. without changing observation geometry. The shapes of the spectra for both polarities are similar, but the peak intensity is consistently lower when the substrate is biased positive, over a range of 2.8 to 4.2 V (Figure 5b). This difference is likely due to absorption of emitted photons by the NAB layer, implying that the photons are generated more efficiently at the

positively biased electrode. Therefore positive polarity causes photoemission "under" the molecular layer, adding the NAB absorbance to that of the eC/Au top contact. If light emission results from hot carriers coupling to surface plasmons, the emission spectrum should depend on the contact material, so $NAB_8$ MJs were made with Au/eC substrates and top contacts of Au only or eC/Au with either 3 nm or 18 nm of eC. Emission spectra for the three different top contact cases biased at -4.3 V are compared in Figure 5c, and do show variation in shape for different top contacts. The Au-only contact exhibits a doublet similar to that reported for AlOx tunnel junctions[21], and this doublet disappears with increasing thickness of eC. As shown in Figure 5d, $hv_{co}$ is linear with bias for both Au and eC/Au as well as with both polarities for Au/eC/$NAB_8$/eC/Au. As already noted in Figure 4, the $eC_3/Au_{20}$ top contact and optical detection equipment are capable of generating and monitoring emitted light from 1.3 to 3.4 eV, which is adequate for the current study.

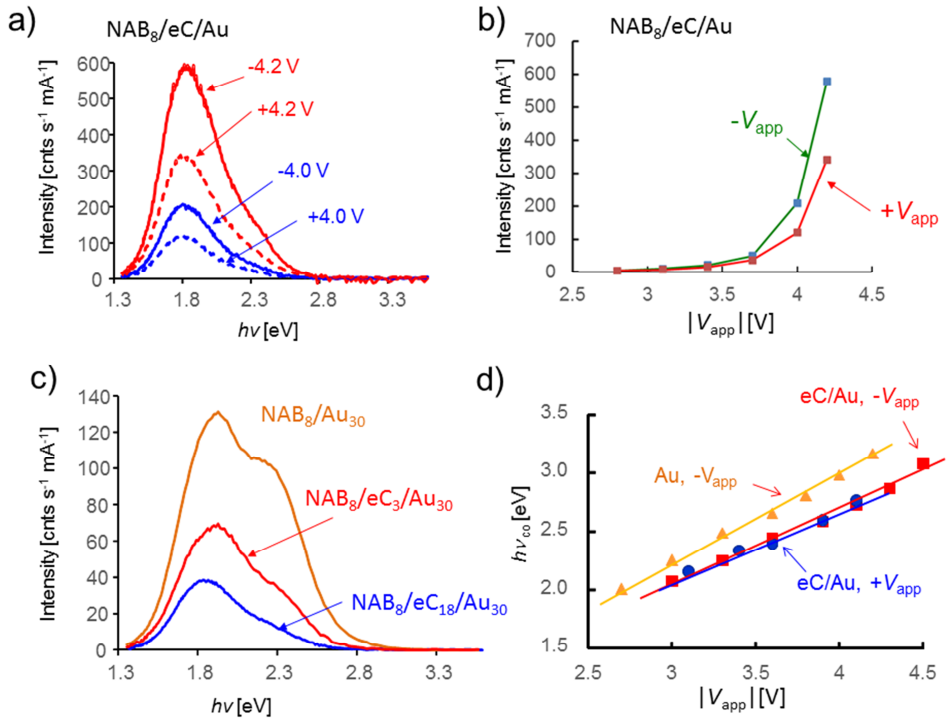


**Figure 5.** a) Emission spectra for a single eC/$NAB_8$/eC MJ biased with both polarities (solid curves- negative bias, dashed curves- positive bias) on the same intensity axis. b) Intensity vs $|V_{app}|$ for the $NAB_8$ MJ at both polarities. c) Emission spectra for $Au_{30}/eC_{10}/NAB_8$/MJs with three different top contacts, as indicated, with $V_{app}$ = -4.3 V. d) Plots of $hv_{co}$ vs $|V_{app}|$ for two different top contacts, as indicated. Both bias polarities (red and blue lines) are shown for the eC/Au top contact.

Additional light emission spectra for four junction structures and thickness range of 8-26 nm are shown in Supporting Information, Figures S4 and S5. **Figure 6a** shows selected spectra for all four molecules, in addition to an azobenzene spectrum presented previously[3a]. Since photon emission reached its maximum at different bias values for different molecules, the spectra are difficult to compare for a single $V_{app}$.

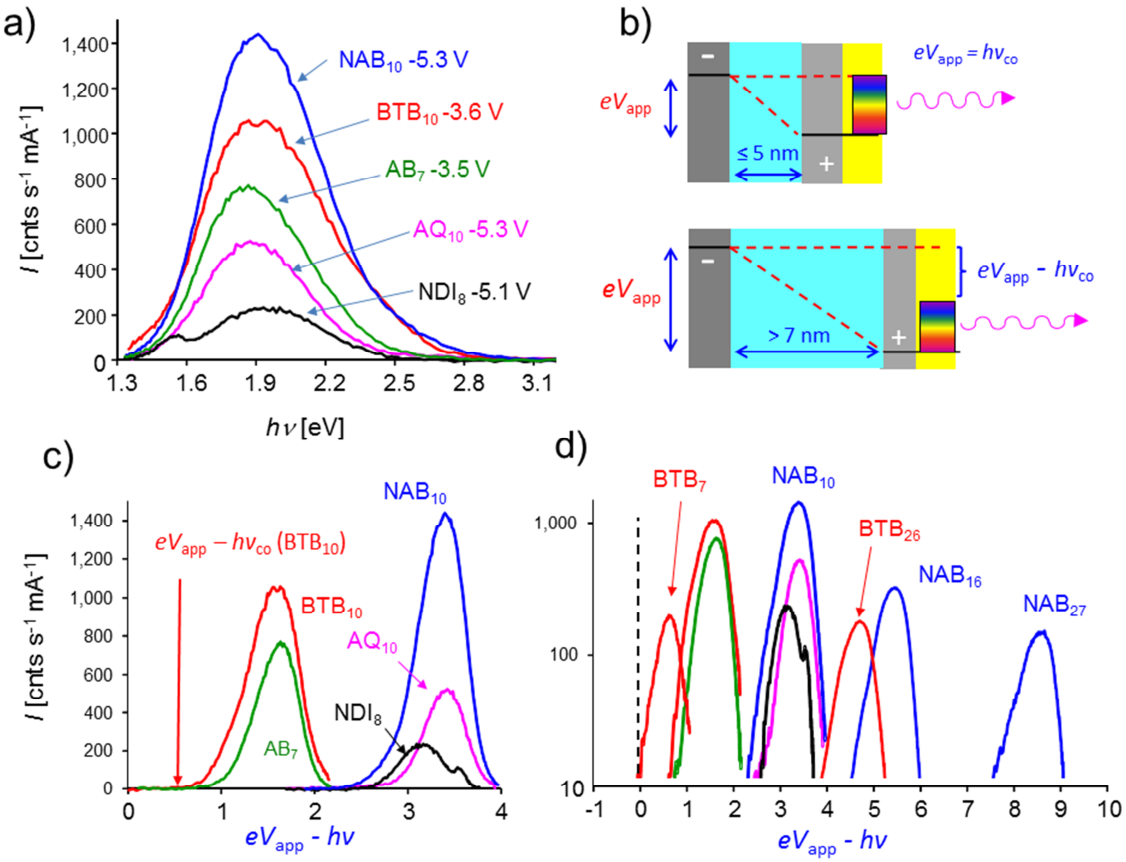


**Figure 6.** a) Emission spectra for eC/molecule/eC junctions with five different molecular structures. All spectra are color coded as BTB (red), NAB (blue), AQ (pink), NDI (black) and Azobenzene (AB, green). b) Schematic energy diagrams showing $eV_{app}$, emitted light, and energy loss for thin (≤ 5nm) and thick (>7 nm) MJs. c) The spectra of panel (a) plotted vs energy loss ≡ $eV_{app} - h\nu$, with the red arrow showing a loss of < 1eV for $BTB_{10}$. d) Composite plot of log(intensity) vs energy loss for additional thicknesses of NAB (blue curves, 10, 16, and 27 nm from left to right) and BTB (blue curves, 7, 10, and 26 nm) showing a range of $eV_{app}$ - $h\nu_{co}$ values from 0 to 9 eV. The left intercept with the detection limit indicates the energy loss for $h\nu_{co,}$ and the vertical dashed line indicates zero energy loss (i.e. $eV_{app} = h\nu_{co}$)

Upon initial inspection of Figure 6a, the emission spectra are qualitatively similar except for NDI which has a reproducible secondary peak at approximately 1.5 eV. The NDI molecule is

fluorescent and exhibits a similar secondary peak at ~1.5 eV when a single NDI molecule acts as a conductor between biased carbon nanotubes[17]. In the present case, this feature may be excited by photons from the hot carrier photoemission at ~2 eV. The similarity of the spectra is consistent with an emission process involving excitation of plasmons in the eC/Au contact by non-equilibrium carriers, which can then decay by emitting photons, as described above. However, the bias required to produce the spectra of Figure 6a varies significantly for different molecules, e.g by ~1.5 V for the case of $BTB_{10}$ and $NAB_{10}$. A more informative parameter for comparing molecules is "energy loss", defined as ($eV_{app} - hv$) and shown in figure 6b, which indicates directly the loss of energy between the applied bias and the emitted photons when *d* exceeds 5-7 nm. Figure 6c shows the spectra of panel (a) replotted vs. $eV_{app} - hv$, which highlights differences in energy loss rather than $hv_{co}$. Note that the spectra reverse direction on the *x*-axis, and clearly emphasize the observed energy loss of the highest energy emitted photon (shown by the red arrow in Figure 6c for the case of $BTB_{10}$). Figure 6d shows a comparison of the same five spectra with those of additional molecular junctions, with energy losses ranging from 0 (vertical dashed line, $eV_{app} = hv$) to 9 eV, and $eV_{app} - hv_{co}$ values from near zero for $BTB_7$ to 7.5 eV for $NAB_{27}$. The advantage of using the "loss" axis is apparent by noting that $NAB_{10}$ with $V_{app}$ = -5.3 V and $BTB_{10}$ with $V_{app}$ =-3.8 V have similar $hv_{co}$ apparent in Figure 6a equal to ~2.8 eV. However, their spectra plotted vs ($eV_{app} - hv$) in 6d are offset significantly, showing energy losses of 0.9 eV for $BTB_{10}$ and 2.3 eV for $NAB_{10}$ for the most energetic emitted photons. The format of Figure 6d provides a direct indication of the effect of molecular layer structure, thickness, and $V_{app}$ on the energy losses between the applied bias and the emitted photon, and permits convenient comparison of different MJs. A complete set of spectra for NAB from *d*=5 to *d*=59 nm is provided in SI Figure S5. As noted above, the emission spectrum is a complex function of the contact materials and other factors, so we rely only on the $hv_{co}$ for deductions about the junction electronic behavior.[3a]

The structure and thickness dependence of $hv_{co}$ are illustrated in **Figure 7** for the four molecules whose *JV* curves were shown in Figure 2, 3 and S1. Figure 7a shows $hv_{co}$ vs $V_{app}$ for NAB junctions ranging in thickness from 5.4 to 59 nm. As noted in our initial report and for many examples of aluminum oxide junctions, direct tunneling is expected to be elastic, as was observed for thin BTB junctions as well as Al/AlOx/Au devices[3a] using the experimental approach described here. As NAB thickness increases above 5 nm, the energy of the emitted light decreases (i.e. $hv_{co} < eV_{app,}$), and for thick molecular layers the difference can be large. For example, 16 V applied across a $NAB_{40}$ junction produced a maximum emitted photon energy of 2.2 eV, indicating an energy loss of 13.8 eV. In all cases, the energy loss increases with increasing bias, except for the elastic cases, and this dependence provides some mechanistic insights as described below in the Discussion section.

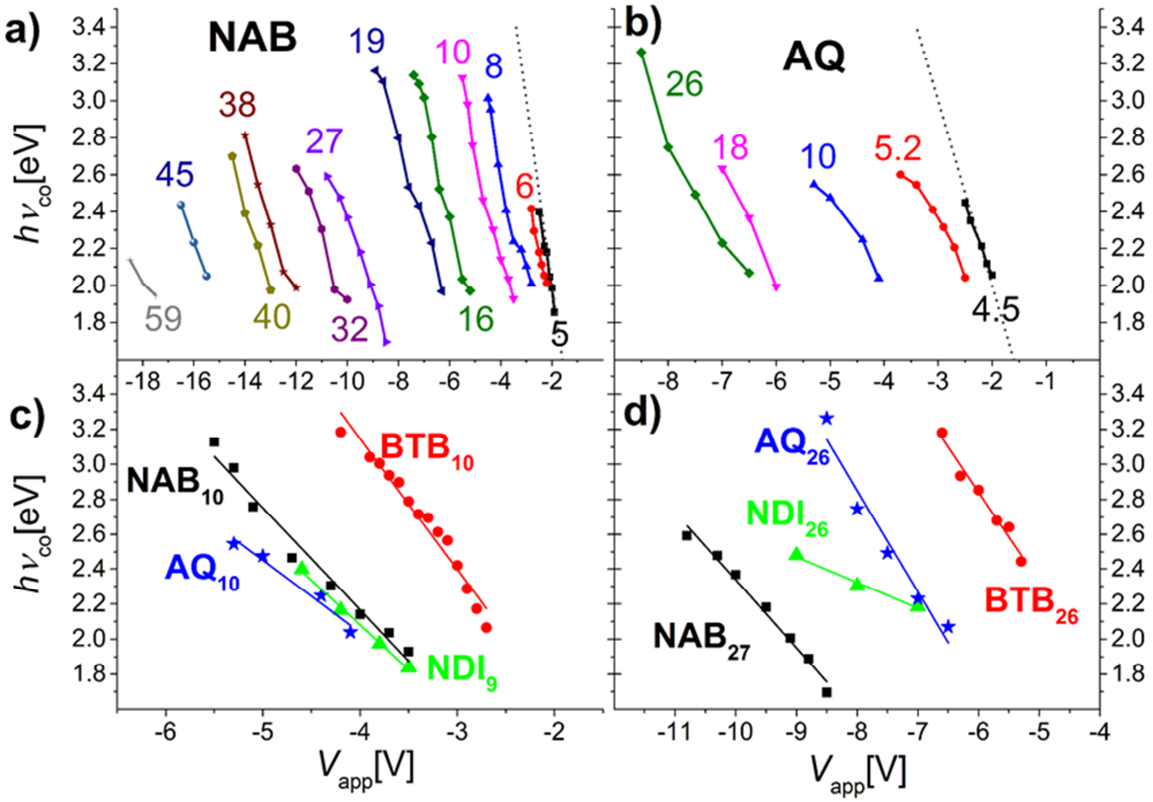


**Figure 7.** a) $hv_{co}$ vs $V_{app}$ for NAB MJs with $d$ = 5 - 59 nm, with numeric labels indicating the thickness of each device in nm. Dashed line indicates elastic case where $hv_{co} = eV_{app}$. b) Similar plot for AQ MJs with $d$ = 4.5 - 26 nm. c) Comparison of 9-10 nm thick MJs of the four molecules, all with negative bias except NDI which was positively biased and plotted here on $-V_{app}$ scale. d) Comparison of 26-27 nm thick MJs for all four molecules.

Figure 7b shows similar plots for AQ devices, which also exhibit an approach to the elastic limit for small *d*, and increasing shifts away from elastic transport as the thickness is increased. Figure 7c and 7d show $h\nu_{co}$ vs $V_{app}$ plots for the junctions of ~10 nm and 26 nm with the *JV* curves shown in Figure 3, to permit comparison of MJs of similar thicknesses. Both the slope and the departure from the elastic line vary significantly between molecular structures, indicating quite different energy losses. For example, emission of a 2.5 eV photon requires $V_{app} \approx 5.2$ V for $BTB_{26}$, ≈ 7.5 V for $AQ_{26}$ and ≈ 10.5 V for $NAB_{27}$, and the range of required bias is > 5V between $BTB_{26}$ and $NAB_{27}$. As shown in **Figure 8**, which plots the energy loss as a function of thickness for four different structures, the loss is approximately linear for all four molecules (although the slopes differ), and this trend extends to greater than 60 nm for NAB and NDI. NAB, AQ, and BTB all reach the elastic limit for 4.5 - 7 nm thick molecular layers, but even the thinnest NDI MJ with *d*= 7.9 nm exhibited energy loss.

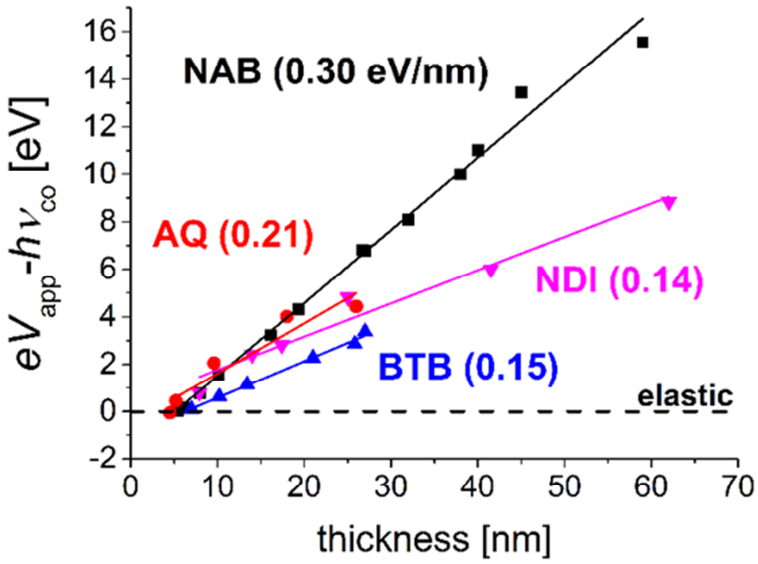


**Figure 8.** Plots of $eV_{app} - h\nu_{co}$ at the onset of light emission for all four molecules, with their slopes indicated. Note that the *x*-axis intercept is similar for all cases, in the range of 4.5-6 nm. Horizontal dashed line indicates elastic transport with zero energy loss.

The focus of the current report is on light emission from molecular junctions and the variables which affect it, rather than a detailed discussion of transport mechanisms in thick diazonium-derived molecular layers. However, a preliminary investigation of the effect temperature on NAB devices was undertaken to assist the interpretation of the light emission results. Past measurements on devices have been carried out from above room temperature to < 10 K for molecular layers less than 5 nm,[4c, 22] and for BTB up to 22 nm.[3b] Here, four NAB junctions were selected that both overlap and extend these previous measurements ($d$ = 3.5, 8.0, 35, and 65 nm) over a 77 – 325 K temperature range. The *JV* behavior of the four NAB junctions at selected temperatures (all in < $10^{-5}$ torr vacuum) are shown in **Figure 9**a.

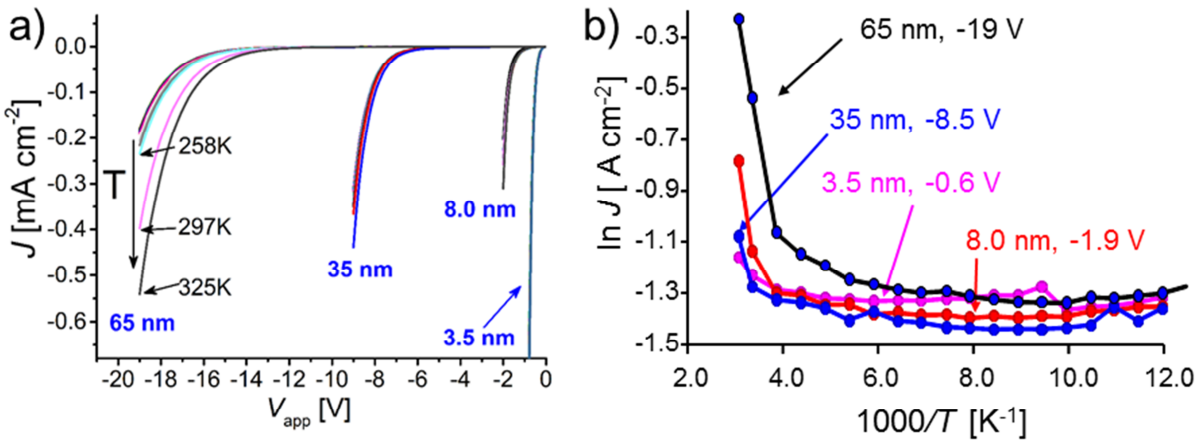


**Figure 9.** a) *JV* curves for negative $V_{app}$ for eC/NAB/eC MJs with the indicated thicknesses between 3.5 and 65 nm. The curves shown are overlays of a range of temperatures between 77 and 325 K. b) Arrhenius plots constructed at the indicated $V_{app}$ for all four thicknesses.

The current density is weakly dependent on temperature for all four thickness below 200 K, with an activated response for $NAB_{65}$ above 200 K. Due to the large variations in current density with thickness, it was not possible to construct Arrhenius plots for the four thicknesses at a single $V_{app}$, but Figure 9b shows *ln J* vs *1000/T* plots at bias values with measurable current densities. Although some linear regions may be present at high *T*, the plots do not exhibit classical Arrhenius behavior, with very

little temperature dependence between 77 and 200 K. **Table 1** lists the apparent activation energies determined from the Arrhenius slopes at low and high T, showing the lack of significant activation.

**Table 1**. Apparent activation energies, $E_{act}$.

| | $NAB_{3.5}$ | $NAB_{8.0}$ | $NAB_{35}$ | $NAB_{65}$ |
|---|---|---|---|---|
| $V_{app}$ [V] | -0.60 | -1.9 | -8.5 | -19 |
| $E_{act}$ [meV], 225- 325 K | 8.9 | 43.5 | 21.0 | 62.3 |
| $E_{act}$ [meV], 100- 200 K | <1 | <1 | 1.4 | 1.7 |

## 3. Discussion

Both the ubiquitous light emitting diodes and their organic equivalent OLEDs depend on recombination of electrons with holes generated by injection of charge from conducting contacts.[23] Light emitting tunnel junctions based on aluminum oxide generate hot carriers in the light emitting contact (usually Au) by tunneling across a thin AlOx layer.[12, 24] These hot carriers then couple to plasmons in the contact which emit light. The current model for light emission by thin ($d$ <5 nm) organic tunnel junctions described in the Introduction assumes similar hot carrier generation by coherent tunneling, then plasmon coupling to produce light.[3a, 18] The main question of the current report is how the hot carrier model changes for MJs with thickness beyond 5 nm, where coherent tunneling is unlikely. A major associated motivation is to use emitted light to probe transport mechanisms, particularly those associated with transport distances beyond the usual limits for coherent tunneling. Several experimental observations support the conclusion that non-equilibrium carriers act to excite light emission from the contact(s). First, the emission spectrum varies with contact composition, all else being constant (Figure 5c). Second, emission spectra are quite similar for different molecules, with only NDI at high bias showing a secondary peak due to luminescence. Third, the emission profile shape and high energy cut-off ($h\nu_{co}$) are similar for both bias polarities in Au/eC/NAB/eC/Au MJs reported here, when both are viewed with the same geometry (Figure 5a,b). This result indicates that

electrons traversing the MJ in either direction (toward or away from the observation point) produce qualitatively similar light emission. However, the decreased intensity for positive bias is likely due to photon absorption by the NAB molecular layer, implying that light emission occurs more efficiently at the positively biased electrode. Fourth, the change in emission spectrum shape for Au and eC/Au contacts (Figure 5c) with increasing eC thickness further implies that light emission may occur from either or both of the Au and eC layers. As discussed previously, black body radiation cannot account for the emission curve shapes and positions, since the required temperatures would destroy the device.[3a]

Although the photon emission profile is expected to vary with contact material, viewing angle, polarization, etc., the only feature used in the current analysis is $h\nu_{co}$. The device structure and observation system are capable of generating and monitoring light in at least the range of 1.4 to 3.4 eV, so a value of $h\nu_{co}$ within that range is a direct indication of the maximum energy of the carriers that reach the contact and stimulate light emission. This statement is supported by the similarity of $h\nu_{co}$ values for a range of bias values for both Au and eC/Au contacts, as well for both bias polarities with eC/Au (Figure 5d). Furthermore, the energy of maximum emission shifts slightly with increasing $V_{app,}$ but the high energy emission depends strongly on $V_{app}$ (Figure 4c). We view the plasmon mediated light emission as a "reporter" for the carrier energy reaching either contact, with the maximum emitted energy indicating the highest energy carrier traversing the junction. The general shape of the emission spectrum depends mainly on the contact material, but $h\nu_{co}$ depends directly on $V_{app}$ and energy losses in the MJ. The plasmonic properties of the light-emitting contact presumably limits the maximum photon energy, but that limit is above the 3.4 eV range apparent in Figures 4, 6, and 7. A critical point to subsequent discussion is that $h\nu_{co}$ indicates the energy *after* the carrier has traversed the molecular junction, since the photon can only be generated when the hot carrier reaches the contact to stimulate light emission.

As shown in Figure 7a and 7b, light emission from the $NAB_{5.5}$ and $AQ_{4.5}$ MJs satisfies the "elastic" condition, meaning that $h\nu_{co} = eV_{app}$. This was also the case for the $BTB_7$ MJ and AlOx devices reported previously,[3a] and for classical studies of Al/AlOx/Au tunnel junctions.[12, 24-25] Therefore, the results strongly support elastic transport when $d$ < 5 nm, with minimal change in energy loss during transport for at least an observable fraction of the carriers traversing the molecular layer. Elastic transport by coherent tunneling is one possibility, and is shown schematically in **Figure 10 a)** and **b).** Molecules are represented by HOMO (blue) and LUMO (red) levels between contacts, in which the filled levels are indicated by gray shading. The horizontal dashed line represents the electrostatic potential profile, assumed to be linear for simplicity.

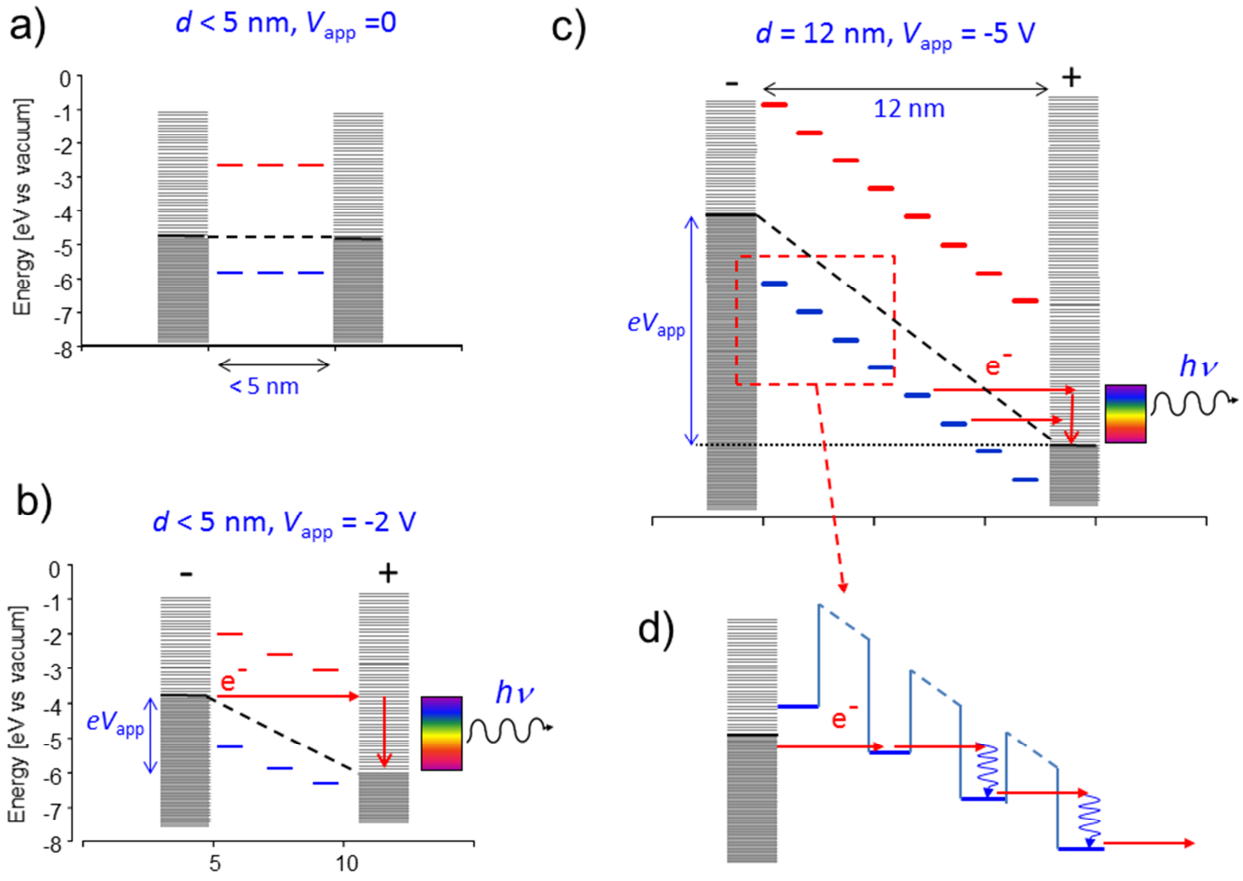


**Figure 10.** a) Schematic energy level diagram of a molecular junction consisting of contacts (gray), HOMO levels (blue) and LUMOs (red) in the molecular layer. Energies are referred to vacuum, with the contact Fermi level equal to -4.8 V. b) Schematic of thin molecular junction under negative bias, with dashed line indicating

the electrostatic potential profile. Horizontal red arrow shows elastic transport followed by emission of light in the positive contact. c) Schematic for 12 nm molecular junction under negative bias, with electron transfers indicated by horizontal red arrows. d) enlargement of molecular layer, as described in the text.

Coherent tunnelling is depicted in Figure 10b for negative bias of the bottom contact, resulting in a hot electron at the top electrode which then stimulates photon emission. In the elastic limit the maximum emitted photon energy ($h\nu_{co}$) equals $eV_{app}$, as observed experimentally for thin (d ~ 5nm) AQ, NAB, and BTB junctions, as well as AlOx[3a][12, 24-25]. The departure of $h\nu_{co}$ from elastic behavior observed for all junctions with $d$ > 5 nm (or *7* nm for BTB) clearly indicates an energy loss somewhere in the system, since the maximum emitted photon energy ($h\nu_{co}$) is significantly smaller than the input energy of $eV_{app}$. Absence of finite loss in some cases and the linearity of the loss with molecular layer thickness rules out parasitic losses in the leads or contacts, as well as significant losses during carrier injection at the electrode/molecule interfaces. Figure S7 in SI shows that variation of eC thickness from 2 to 25 nm in the top contact had minimal effect on either the *JV* response or $h\nu_{co}$, thus ruling out significant ohmic losses inside the carbon films. Classical inelastic scattering in conductors and insulators is generally exponential with distance, whereas the losses apparent in Figure 8 are linear with thickness. Note that the slopes shown in Figure 8 (0.14 – 0.30 eV/nm) are similar in magnitude to the applied electric fields assuming a linear potential profile (~0.2 to 0.3 V/nm). We conclude from the results that energy loss occurs within the molecular layer, and is associated with incoherent carrier transport, likely involving multiple steps. Figure 10c shows schematic energy levels for a 12 nm molecular layer, with the HOMO and LUMO levels shifted in accordance with the applied electric field. Note that the HOMO levels represent molecular orbitals which are separated from each other by a tunnelling barrier, such as might result from non-planar dihedral angles between molecular subunits. Although coherent tunnelling across 12 nm is unreasonable, electrons may transfer to empty contact orbitals by either tunneling or field ionization[3b], as shown by the red arrows. Based on the experimental results, such transport is possible for distances less than 5-7 nm, and result in a hot carrier

in a contact. As indicated in figure 10c there may be more than one HOMO which can transfer electrons to the positively biased contact, resulting in photons of lower energy, but the maximum photon energy is determined by the orbital at the limit of elastic transport. As a result, $h\nu_{co}$ is less than $eV_{app}$ for junctions thicker than 5-7 nm. Figure 10d shows a possible mechanism for transport within the organic layer subsequent to the initial hot electron generation. A cascade of tunneling events followed by thermal relaxation would allow electrons to traverse the film to fill the hole left behind by the hot electron. These could be inelastic tunneling events [12, 26] or coherent tunneling followed by vibrational relaxation, but in either case they result in an energy loss for each "step". Furthermore, this energy loss increases with $V_{app}$ (as shown in Figure 7) if the number of "steps" stays constant. The model of figure 10 and the experimental observations are consistent with an approximately linear potential distribution in the organic layer, but not with significant potential losses as the eC/molecule interfaces.

Extensive research on transport through organic films much thicker than those examined here (generally $d$ > 100 nm), has resulted in a collection of "hopping" models based on a sequence of discrete steps, for example between conductive regions in a conducting polymer such as polythiophene.[27] Several of these models involve activated, Marcus-like electron transfer reactions and among those is "redox exchange" in which transport occurs by a series of electron transfers in a redox or conducting polymer.[28] At least for NAB, the small activation energies of Figure 9 and Table 1 rule out Marcus-like electron transfer, since typical $E_{act}$ values for reorganization exceed 200 meV. It is important to note that although the small $E_{act}$ values rule out significant reorganization *preceding* electron transport, structural changes or fluctuations *after* transport are still possible, with the energy dissipated in the matrix. The current results on four molecules demonstrate that inelastic, weakly activated (at least for NAB and BTB) transport can occur across distances of 6-62 nm, with an accompanying energy loss that depends on molecular structure. Research is ongoing into transport

mechanisms beyond the ~5 nm limit normally observed for elastic transport, and we anticipate that light emission and associated energy losses will provide valuable evidence for elucidating transport mechanism.

## 4. Conclusions

Carbon based molecular junctions with molecular layer thicknesses of 5-59 nm emit light under bias, with the spectrum and its intensity varying with molecular layer structure and thickness. Light is generated when a "hot" carrier arrives at the molecule/contact interface, then couples to surface plasmons in the contact. Junction current is symmetric with respect to bias polarity, with slightly weaker light emission for positive bias indicating that light emission occurs predominantly at the positively biased contact, with the molecular layer absorbing some of the light when the bottom contact is positive. The shape of the emission spectrum is largely determined by the properties of the contacts rather than the molecules, however the maximum emitted photon energy ($h\nu_{co}$) is limited to the applied bias, i.e. $eV_{app}$. Hence $h\nu_{co}$ indicates energy losses during transport through the junction, with elastic transport corresponding to the case where $h\nu_{co} = eV_{app}$. For AQ and NAB molecular layers, the elastic condition is satisfied for films less than 5 nm thick, and for BTB up to 7 nm. For thicker films of all molecules examined, $h\nu_{co} < eV_{app}$, and the energy loss is linear with molecular layer thickness. The observed energy loss is strongly dependent on molecular structure, for example varying by ~5 eV for the four different structures and $d$ = 26 nm (Figure 6d and 7d). The *JV* behavior for NAB devices is weakly dependent on temperature, with an apparent activation energy of less than 2 meV for $d$ = 3.3 to 65 nm and $T$ = 100 to 200 K. The results clearly indicate inelastic transport for films thicker than 5 nm, although they are not consistent with either redox exchange or classical inelastic scattering mechanisms. The near-zero Arrhenius slopes for a wide range of molecular layer thickness clearly indicate that thermally induced reorganization preceding electron transfer is unnecessary, but do not

rule out energy transfer to the matrix following electron transfer. A probable transport mechanism for *d* > 5 nm involves multiple steps down an approximately linear potential profile, with energy losses by inelastic tunneling or vibrational relaxation. The ability to determine carrier energy upon arrival at the second contact/molecule interface should prove valuable for determining transport mechanism across 5-60 nm distances, and ways to control transport by variation of molecular structure.

**5. Experimental Section**

Light emission was monitored with an Olympus BX60 microscope and fiber optic output coupled to an Andor Solis spectrograph with an Andor Newton DU-920N CCD cooled to -60 °C. Samples were mounted on a custom-built sample holder with 4 probes for applying an external bias using a Keithley 2602a in a DC mode. A Keithley 2602a was connected to the sample stage throughout the experiment, *i.e.,* for initial and final *i*-*V* curve measurements as well as for DC bias application. After electrical connection, samples were aligned in the microscope stage and focused using a 50x, NA=0.45 objective (where the field of view was approximately the same as the junction area) and an *i*-*V* curve was acquired with a Keithley 2602a to verify contact and ensure a non-shorted sample. An opaque screen was used to isolate the stage from external ambient background light. Acquisition of light consisted of the measurement of a background with no bias applied to the sample. The following spectra were measured at a constant bias ($V_{app}$), starting at low initial bias values to verify the absence of emission at $V_{app} < V_{onset}$. Acquisition was performed using 4 accumulations of 7.5 s with a 50 kHz readout rate, a preamplifier gain of 4x, full vertical binning, and 8 pixel horizontal binning. Intermediate measurements of *i*-*V* curves were conducted to verify sample function. Selected spectra were corrected for the spectrometer response function according the procedure described in SI section 5and are shown in Figure S6 for all four junction types. The response correction had the greatest effect on the low-energy regions of the spectra, but had a minor effect (typically <0.1 eV) on the observed

$h\nu_{co}$. All $h\nu_{co}$ values reported were determined with uncorrected spectra, in part to reduce noise. Maximum photon energy, $h\nu_{co}$ values and their uncertainties were determined by the procedure described in SI section 6 and Figure S7.

Junctions were prepared as described previously,[3a] with the general structure of $Au_{30}/eC_{10}/Mol_x/eC_3/Au_{20}$. Details regarding molecular layer and contact deposition specific to the current report are provided in SI section 8. *J-V* curves measurements and DC bias application were performed using a Keithley 2602a SourceMeter in a four probe configuration[29] to minimize contact resistance errors. *JV* curves were collected starting from 0 V, sweeping towards positive or negative direction to reach limiting current density of ca. ± 30 A/cm$^2$. Notably, most of the junctions were able to tolerate higher current densities, up to 100 A/cm$^2$ using fast scans, but *JV* curves measured with the limiting current of ± 30 A/cm$^2$ provided sufficient information and intact junctions for further light emission measurements. 100 data points, with NPLC 0.001, and filter 10 were used for each polarity measurement, with a nominal duration 0.1 s to avoid junction breakdown. Temperature dependent measurements were performed similarly using Keithley 2602a, connected to a vacuum chamber with liquid nitrogen cooling. Base pressure during data accumulation was 1-2 $\times 10^{-6}$ mbar. Measurement started at 77 K followed by slow heating up to room temperature, using a Scientific Instruments 9700 temperature controller. At each temperature the sample was allowed to stabilize for ca. 5 min before *JV* curves were recorded.

*JV* curves obtained before and after light emission had similar shapes. A single light emission measurement at a lower bias, close to the onset of light emission, did not affect the current density of the junction. Extensive measurement at increased biases (> 2 V higher than onset voltage) for 3-5 min caused a decrease in current density by 50-90%. If significant DC bias caused junction breakdown due to short circuit, light emission terminated, confirming that light generation cannot proceed in the presence of direct short between the contacts.

**Supporting Information**
Supporting Information is available from the Wiley Online Library or from the authors.

**Acknowledgements**
This work was supported by the University of Alberta, the National Research Council of Canada, the National Science and Engineering Research Council and Alberta Innovates Technology Futures. We thank Amin Morteza Najarian, Mykola Kondratenko, Akhtar Bayat and Jerry Alfred Fereiro for the synthesis of diazonium salts used for fabrication of MJs and Prof. Jean-Christophe Lacroix of the University of Paris for providing the BTB amine precursor used to prepare BTB molecular junctions.

Received: ((will be filled in by the editorial staff))
Revised: ((will be filled in by the editorial staff))
Published online: ((will be filled in by the editorial staff))

**Light emission by carbon-based molecular junctions** reveals energy lost during transport as the difference between the applied bias and the maximum emitted photon energy. For molecular layers less than 5 nm thick, transport is elastic, while thicker films show energy losses which are linearly dependent on layer thickness.

Oleksii Ivashenko, Adam Johan Bergren*, and Richard L. McCreery*

**Monitoring of Energy Conservation and Losses in Molecular Junctions through Characterization of Light Emission**

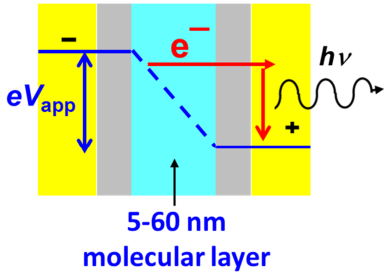


## References

[1] a) R. M. Metzger, *Chem. Rev.* **2015**, *115*, 5056; b) N. Amdursky, D. Marchak, L. Sepunaru, I. Pecht, M. Sheves, D. Cahen, *Adv. Mater.* **2014**, *26*, 7142; c) R. L. McCreery, A. J. Bergren, *Adv. Mater.* **2009**, *21*, 4303; d) A. Vilan, O. Yaffe, A. Biller, A. Salomon, A. Kahn, D. Cahen, *Adv. Mater.* **2010**, *22*, 140; e) A. Salomon, D. Cahen, S. Lindsay, J. Tomfohr, V. B. Engelkes, C. D. Frisbie, *Adv. Mater.* **2003**, *15*, 1881; f) J. R. Heath, *Annual Review of Materials Research* **2009**, *39*, 1; g) P. Song, C. S. S. Sangeeth, D. Thompson, W. Du, K. P. Loh, C. A. Nijhuis, *Adv. Mater.* **2016**, *28*, 631; h) A. Wan, C. S. Suchand Sangeeth, L. Wang, L. Yuan, L. Jiang, C. A. Nijhuis, *Nanoscale* **2015**, *7*, 19547.

[2] A. J. Bergren, L. Zeer-Wanklyn, M. Semple, N. Pekas, B. Szeto, R. L. McCreery, *J. Phys.: Condens. Matter* **2016**, *28*, 094011.

[3] a) O. Ivashenko, A. J. Bergren, R. L. McCreery, *J. Am. Chem. Soc.* **2016**, *138*, 722; b) H. Yan, A. J. Bergren, R. McCreery, M. L. Della Rocca, P. Martin, P. Lafarge, J. C. Lacroix, *Proc. Natl. Acad. Sci. U.S.A.* **2013**, *110*, 5326.

[4] a) S. H. Choi, B. Kim, C. D. Frisbie, *Science* **2008**, *320*, 1482; b) H. B. Akkerman, R. C. G. Naber, B. Jongbloed, P. A. van Hal, P. W. M. Blom, D. M. de Leeuw, B. de Boer, *Proc. Natl. Acad. Sci. U.S.A.* **2007**, *104*, 11161; c) A. J. Bergren, R. L. McCreery, S. R. Stoyanov, S. Gusarov, A. Kovalenko, *J. Phys. Chem. C* **2010**, *114*, 15806; d) V. B. Engelkes, J. M. Beebe, C. D. Frisbie, *J. Am. Chem. Soc.* **2004**, *126*, 14287; e) R. Har-Lavan, O. Yaffe, P. Joshi, R. Kazaz, H. Cohen, D. Cahen, *AIP Adv.* **2012**, *2*, 012164.

[5] S. H. Choi, C. Risko, M. C. R. Delgado, B. Kim, J.-L. Bredas, C. D. Frisbie, *J. Am. Chem. Soc.* **2010**, *132*, 4358.

[6] a) M. L. Brongersma, N. J. Halas, P. Nordlander, *Nat. Nanotechnol.* **2015**, *10*, 25; b) S. A. DiBenedetto, A. Facchetti, M. A. Ratner, T. J. Marks, *J. Am. Chem. Soc.* **2009**, *131*, 7158.

[7] S. Mukherjee, L. Zhou, A. M. Goodman, N. Large, C. Ayala-Orozco, Y. Zhang, P. Nordlander, N. J. Halas, *J. Am. Chem. Soc.* **2014**, *136*, 64.
[8] K. Turvey, J. W. Allen, *J. Phys. C: Solid State Phys.* **1973**, *6*, 2887.
[9] a) P. D. Sparks, J. E. Rutledge, *Phys. Rev. B* **1989**, *40*, 7574; b) A. M. Goodman, *Phys. Rev.* **1966**, *144*, 588; c) A. M. Goodman, *J. Appl. Phys.* **1970**, *41*, 2176.
[10] V. V. Afanas′ev, *Internal Photoemission Spectroscopy: Principles and Applications*, Elsevier Science, Oxford, UK 2008.
[11] a) J. A. Fereiro, M. Kondratenko, A. J. Bergren, R. L. McCreery, *J. Am. Chem. Soc.* **2015**, *137*, 1296; b) J. A. Fereiro, R. L. McCreery, A. J. Bergren, *J. Am. Chem. Soc.* **2013**, *135*, 9584.
[12] J. Lambe, S. L. McCarthy, *Phys. Rev. Lett.* **1976**, *37*, 923.
[13] A. Yu, S. Li, G. Czap, W. Ho, *Nano Lett.* **2016,** DOI: 10.1021/acs.nanolett.6b01824.
[14] a) E. Flaxer, O. Sneh, O. Cheshnovsky, *Science* **1993**, *262*, 2012; b) D. Fujita, T. Ohgi, W. L. Deng, K. Ishige, T. Okamoto, S. Yokoyama, T. Kamikado, S. Mashiko, *Surf. Sci.* **2001**, *493*, 702; c) G. Hoffmann, L. Libioulle, R. Berndt, *Phys. Rev. B* **2002**, *65*.
[15] a) Z. C. Dong, X. L. Guo, A. S. Trifonov, P. S. Dorozhkin, K. Miki, K. Kimura, S. Yokoyama, S. Mashiko, *Phys. Rev. Lett.* **2004**, *92*, 086801; b) F. Rossel, M. Pivetta, W. D. Schneider, *Surf. Sci. Reports* **2010**, *65*, 129.
[16] T. Shamai, Y. Selzer, *Chem. Soc. Rev.* **2011**, *40*, 2293.
[17] C. W. Marquardt, S. Grunder, A. Błaszczyk, S. Dehm, F. Hennrich, H. V. Löhneysen, M. Mayor, R. Krupke, *Nat. Nanotechnol.* **2010**, *5*, 863.
[18] W. Du, T. Wang, H.-S. Chu, L. Wu, R. Liu, S. Sun, W. K. Phua, L. Wang, N. Tomczak, C. A. Nijhuis, *Nature Photonics* **2016**, *10*, 274.
[19] a) S. Y. Sayed, A. Bayat, M. Kondratenko, Y. Leroux, P. Hapiot, R. L. McCreery, *J. Am. Chem. Soc.* **2013**, *135*, 12972; b) R. McCreery, H. Yan, A. J. Bergren, *Phys. Chem. Chem. Phys.* **2013**, *15*, 1065; c) S. Y. Sayed, J. A. Fereiro, H. Yan, R. L. McCreery, A. J. Bergren, *Proc. Natl. Acad. Sci. U.S.A.* **2012**, *109*, 11498.
[20] H. Yan, A. J. Bergren, R. L. McCreery, *J. Am. Chem. Soc.* **2011**, *133*, 19168.
[21] a) A. J. L. Ferguson, P. Dawson, D. G. Walmsley, *J. Phys.: Condens. Matter* **1989**, *1*, 9021; b) P. Dawson, D. G. Walmsley, H. A. Quinn, A. J. L. Ferguson, *Phys. Rev. B* **1984**, *30*, 3164.
[22] A. M. Mahmoud, A. J. Bergren, N. Pekas, R. L. McCreery, *Adv. Funct. Mater.* **2011**, *21*, 2273.
[23] a) T. Sengoku, T. Yamao, S. Hotta, *Journal of Non-Crystalline Solids* **2012**, *358*, 2525; b) C. Fan, C. Yang, *Chem. Soc. Rev.* **2014**, *43*, 6439; c) J.-H. Jou, S. Kumar, A. Agrawal, T.-H. Li, S. Sahoo, *Journal of Materials Chemistry C* **2015**, *3*, 2974; d) X. Yang, G. Zhou, W.-Y. Wong, *Chem. Soc. Rev.* **2015**, *44*, 8484.
[24] a) S. L. McCarthy, J. Lambe, *Appl. Phys. Lett.* **1978**, *33*, 858; b) J. R. Kirtley, T. N. Theis, J. C. Tsang, *Appl. Phys. Lett.* **1980**, *37*, 436; c) J. Kirtley, T. N. Theis, J. C. Tsang, *Phys. Rev. B* **1981**, *24*, 5650.
[25] T. N. Theis, J. R. Kirtley, D. J. DiMaria, D. W. Dong, *Phys. Rev. Lett.* **1983**, *50*, 750.
[26] R. Berndt, J. K. Gimzewski, P. Johansson, *Phys. Rev. Lett.* **1991**, *67*, 3796.
[27] a) J. C. Lacroix, K. I. Chane-Ching, F. Maquere, F. Maurel, *J. Am. Chem. Soc.* **2006**, *128*, 7264; b) E. Johansson, S. Larsson, *Syn. Met.* **2004**, *144*, 183; c) A. S. Dhoot, G. M. Wang, D. Moses, A. J. Heeger, *Phys. Rev. Lett.* **2006**, *96*, 246403.
[28] a) R. H. Terrill, R. W. Murray, in *Molecular Electronics*, (Eds: J. Jortner, M. Ratner), Blackwell Science Ltd., 1997, 215; b) S. Ranganathan, R. W. Murray, *J. Phys. Chem. B* **2004**, *108*, 19982; c) D. A. Buttry, F. C. Anson, *J. Am. Chem. Soc.* **1983**, *105*, 685.
[29] A. J. Bergren, R. L. McCreery, *Annu. Rev. Anal. Chem.* **2011**, *4*, 173.

# Supporting Information

**Monitoring of Energy Conservation and Losses in Molecular Junctions through Characterization of Light Emission**

*Oleksii Ivashenko, Adam Johan Bergren, and Richard L. McCreery*[*]

Dr. O. Ivashenko, Prof. R. L. McCreery
University of Alberta, 11421 Saskatchewan Dr. Edmonton, AB T6G 2M9, Canada
E-mail: McCreery@ualberta.ca

Dr. A. J. Bergren, Prof. R. L. McCreery
National Institute for Nanotechnology, 11421 Saskatchewan Dr. Edmonton, AB T6G 2M9, Canada
E-mail: Adam.Bergren@nrc.ca

**Content:**

## 1. Complete sets of JV curves

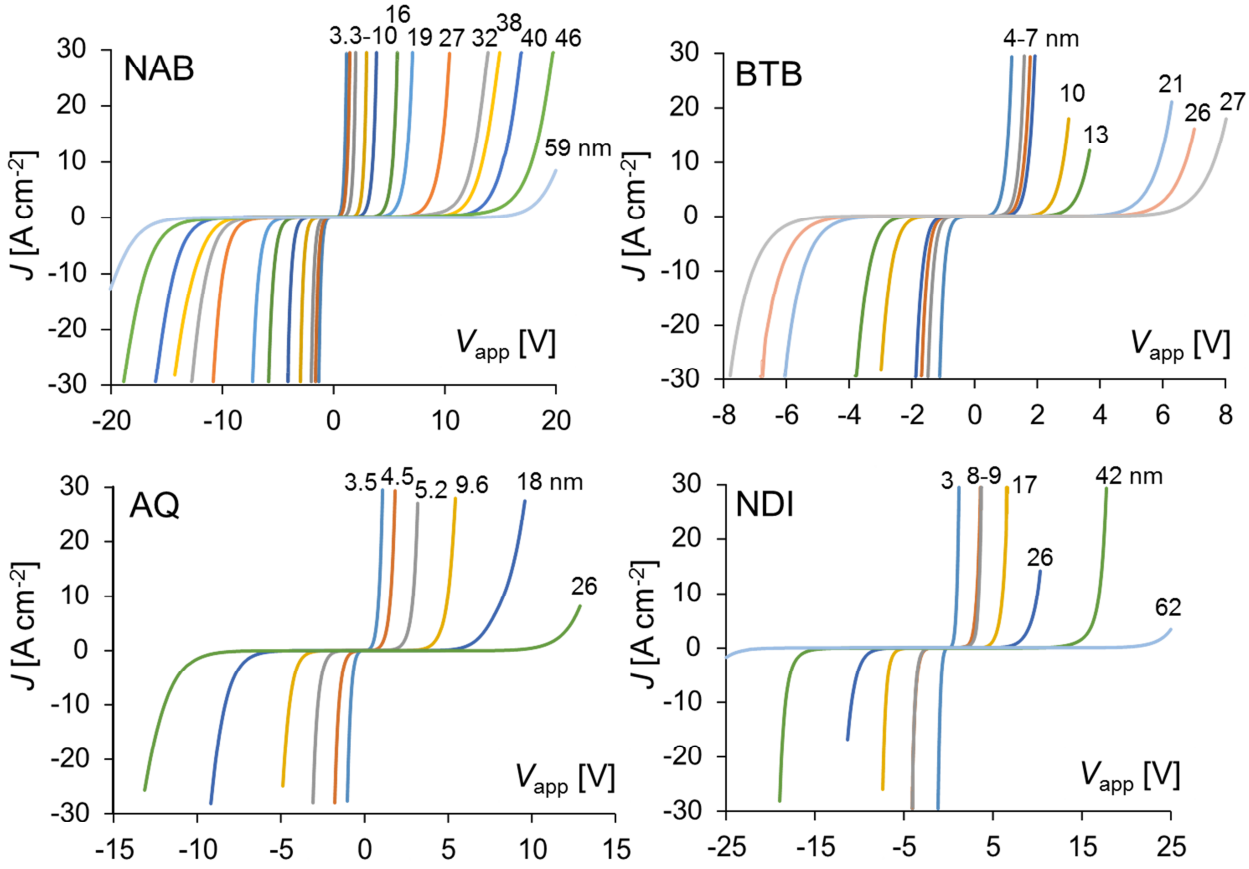


**Figure S1.** *JV* curves for $Au_{30}/eC_{10}/Mol_x/eC_3/Au_{20}$ MJs containing the indicated molecules, with the numbers on each curve denoting molecular layer thickness in nm. In all cases, $V_{app}$ was initiated at 0 volts with a Keithley 2602 source-measurement unit, and required < 1 second for data acquisition. The polarity of $V_{app}$ is the bottom Au contact relative to the top, with subsequent light emission observed from the top (20 nm) Au contact.

## 2. Al/AlOx/eC/Au emission spectra

In part to characterize the effects of the eC/Au top contact on light emission, complete spectra for $Al/AlOx/eC_3/Al_{20}$ are provided in figure S2, using the same apparatus and conditions as the spectra of molecular junctions.

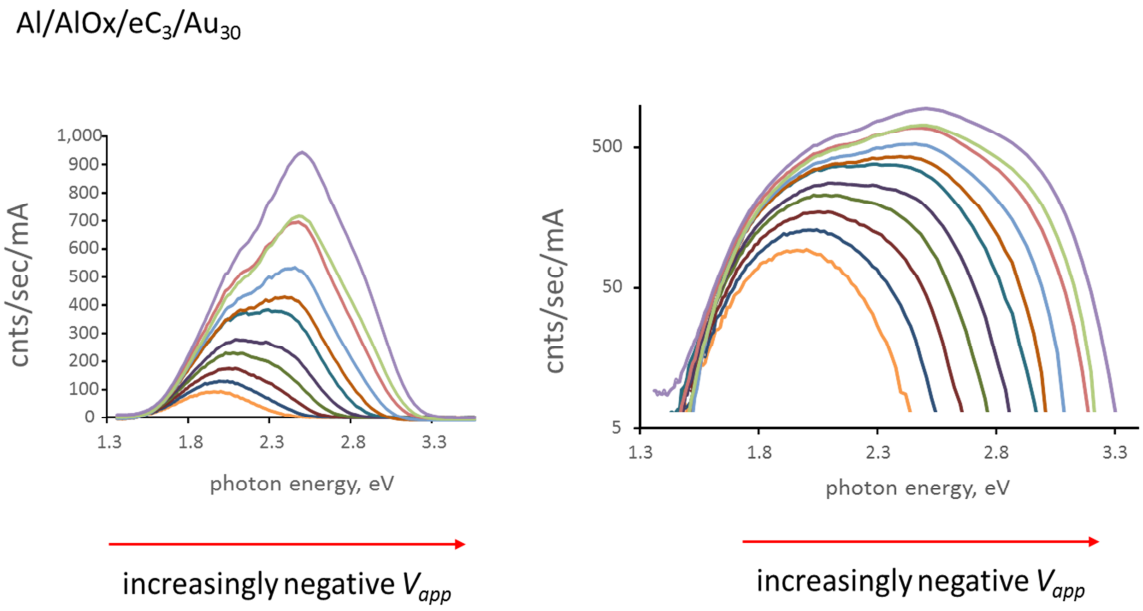


**Figure S2.** Uncorrected emission spectra of an Al/AlOx/$eC_3$/$Al_{20}$ junction on linear (left) and log (right) intensity scales. Applied bias for spectra in both plots from left to right was -2.1, -2.2, -2.4, then to -3.4 V in 0.1 V increments.

### 3. Symmetry of JV responses

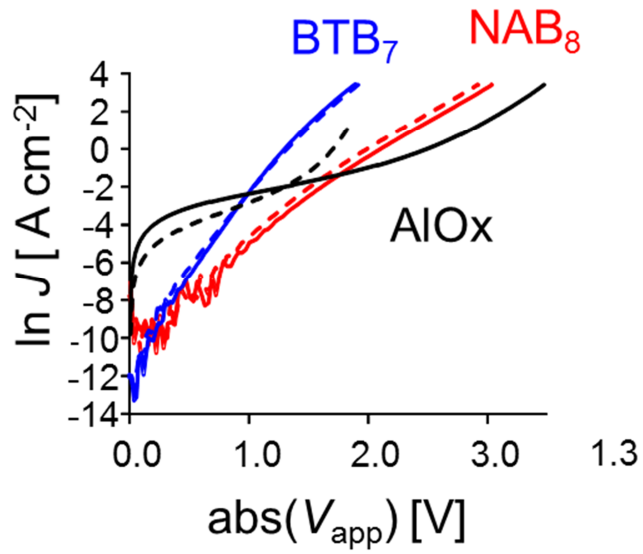


**Figure S3.** JV responses plotted vs absolute bias voltage to permit comparison of positive (dashed) and negative (solid line) polarities. Curves are nearly symmetric for NAB and BTB, while Al/AlOx departs from symmetric response due to breakdown when the Al is biased positive.

## 4. Additional light emission spectra

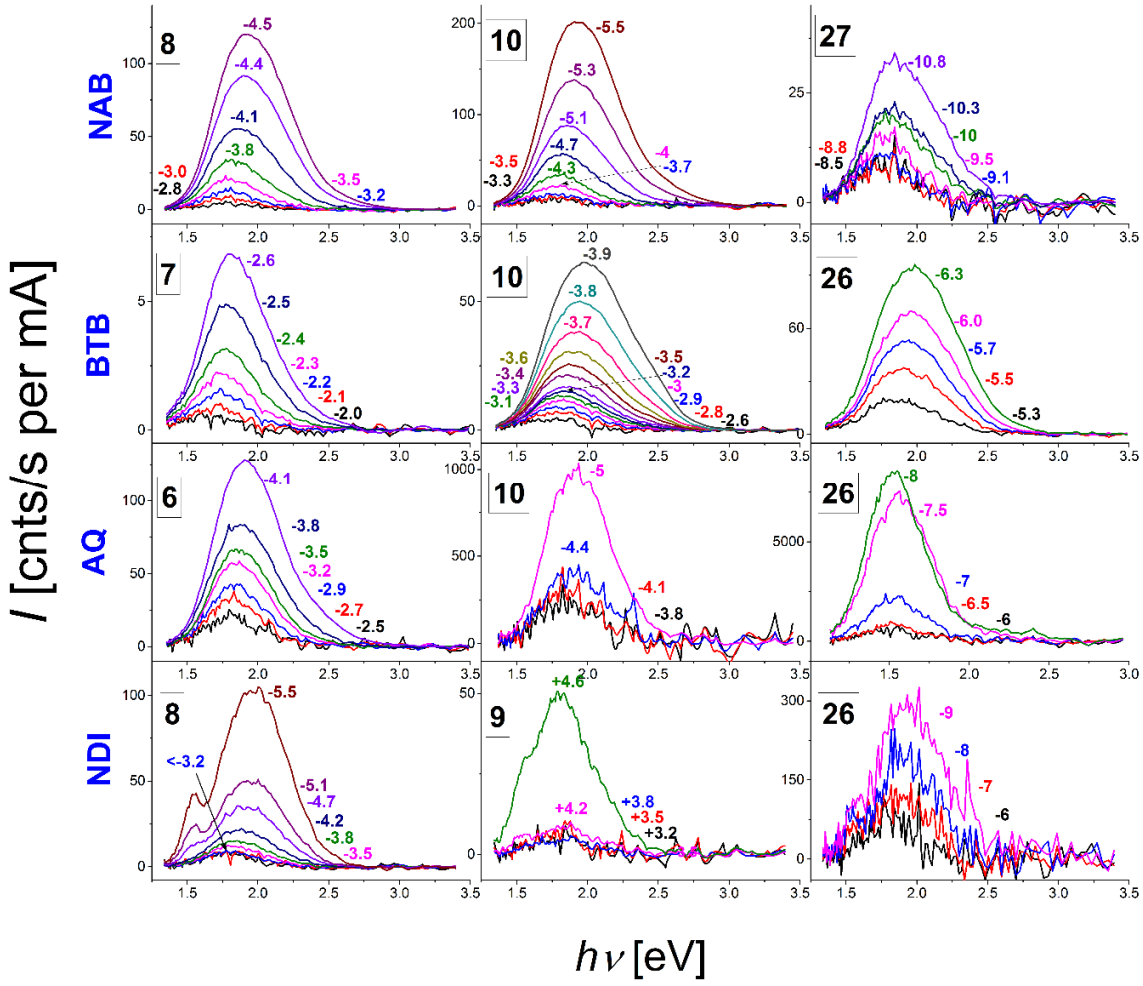


**Figure S4.** Additional uncorrected spectra of light emission for NAB, BTB, AQ and NDI junctions with thickness 6-8 nm (first column), 9-10 nm (second column) and 26-27 nm (third column) with thickness indicated in the left upper corner of each panel. Applied DC bias is indicated next to each curve, all junctions were measured in negative polarity, except $NDI_9$ which was measured with a positive bias. Each curve was normalized for the current flowing through the device.

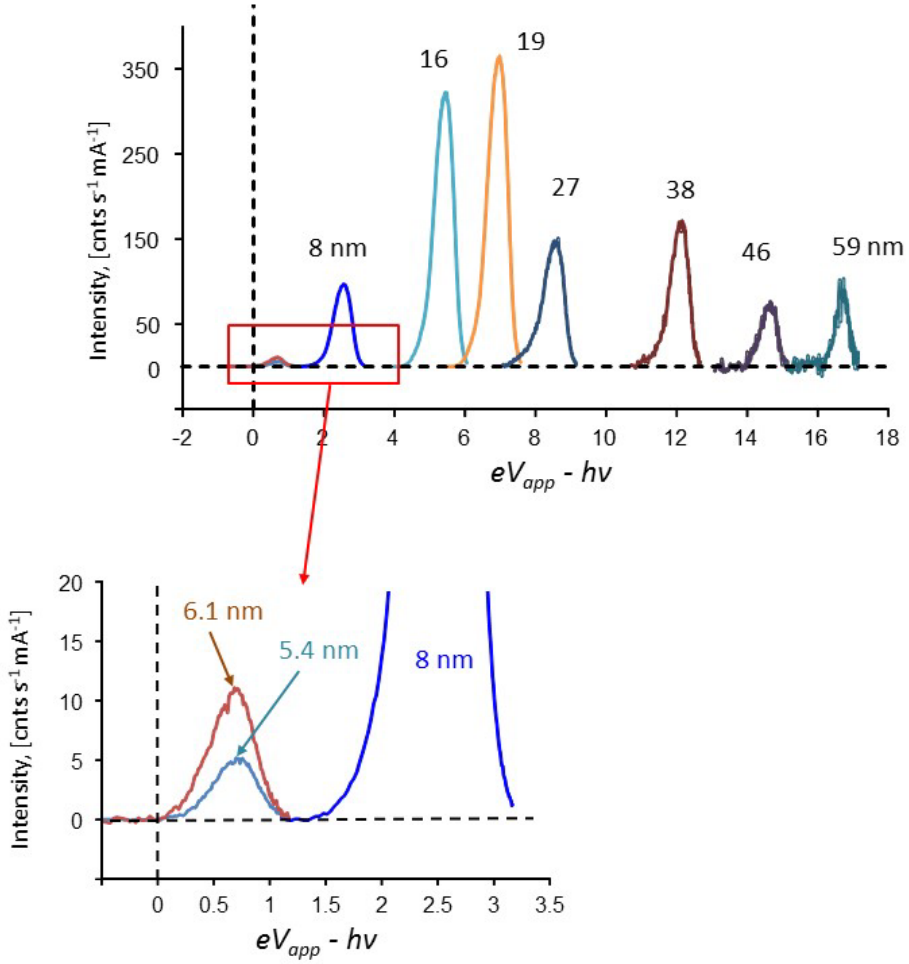


**Figure S5.** Emission spectra for $Au_{30}/eC_{10}/NAB/eC_3/Au_{20}$ junctions with NAB thicknesses from 5 to 59 nm, plotted vs. energy loss in order to separate the nine spectra. Photon energy cutoff values ($h\nu_{co}$) from these spectra are plotted in figure 7a of the main text.

**5. Spectral response correction**

In order to account for the variable sensitivity of the CCD detector in the range 300-900 nm, a correction for the spectrometer response function was carried out using the procedure described previously.[1] The main motivations for this procedure were to obtain an accurate emission spectrum of the light emission and to determine if that affects determination of cut-off energies and corresponding losses.

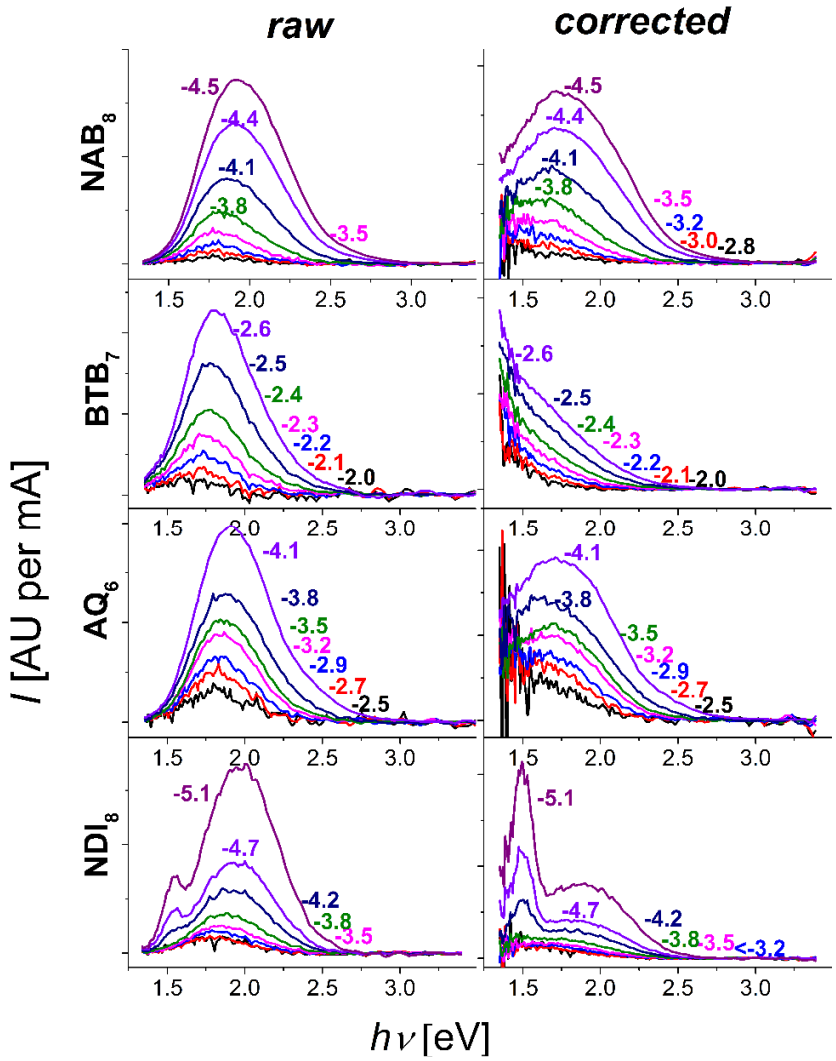


**Figure S6.** Raw (left panels) and corrected for spectrometer response (right panels) light emission spectra for NAB, BTB, AQ, NDI junctions of 6-8 nm thickness.

## 6. Maximum photon energy error analysis

The error in the high energy emission cut-off values reported in the main text were determined by extrapolating a line to the *x*-axis using the first 20 data points above 3σ, where σ is the standard deviation of "dark" response of the CCD. As described elsewhere,[2] the error in the slope and intercept of the line is used to determine the error in the extrapolated *x*-axis intercept by propagation of error. Two examples are shown in **Figure S3a** that illustrate an error of <5% for cases where the emission signal is strong. In the case of weak emission or low photon energy that produce a signal with insufficient data points (i.e., less than 20), the cut-off value was determined as the energy at which the signal exceeds 3σ above the dark signal. As is apparent in **Figure S3b**, the error near the emission threshold is 10-15%. As noted in the main text, the larger error of ~15% occurs for thin molecular junctions and low $V_{app}$, which produces photons of < 2 eV energy detected less efficiently by the silicon CCD detector.

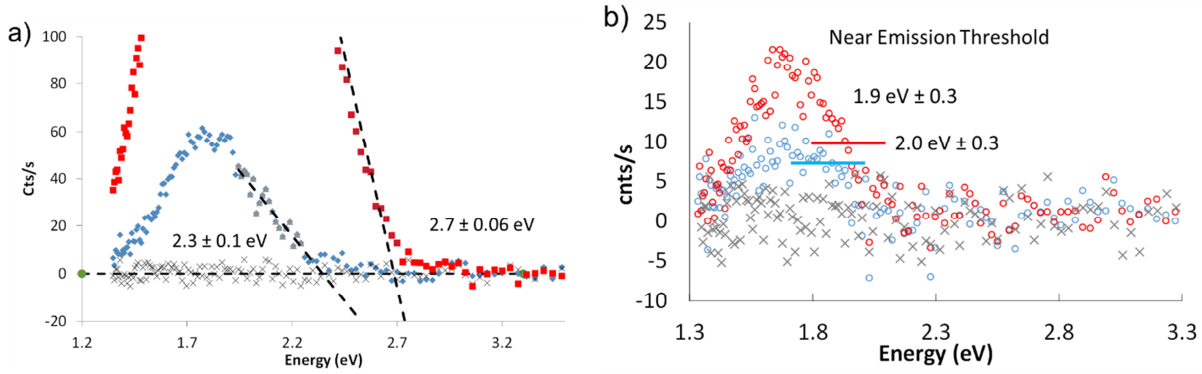


**Figure S7.** a) Illustration of the method used to determine the error in the *x*-intercept of the emission curves for a 10 nm BTB device with 2.9 V applied (blue curve) and 3.4 V applied (red curve). Here, the error values are less than 5%. b) Examples of intercepts near threshold emission for NAB 5.4 nm with applied voltages of 1.9 V (blue curve) and 2.0 V (red curve), showing that the uncertainty in the *x*-axis intercept can increase to ~15%.

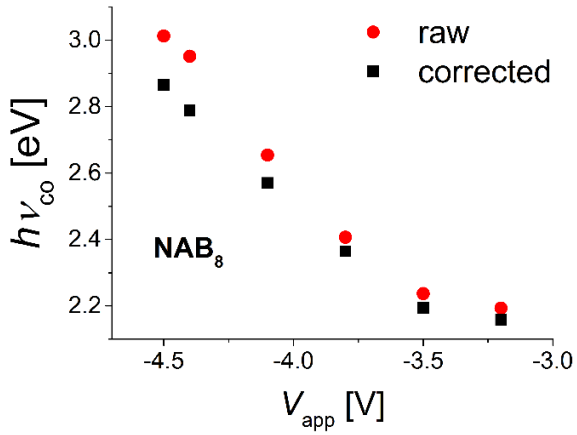


**Figure S8.** Cut-off energy determined using raw (red circles) and corrected (black squares) spectra, showing that cut-off values of corrected spectra are on average 0.1 eV lower.

## 7. Thickness variation for eC contacts

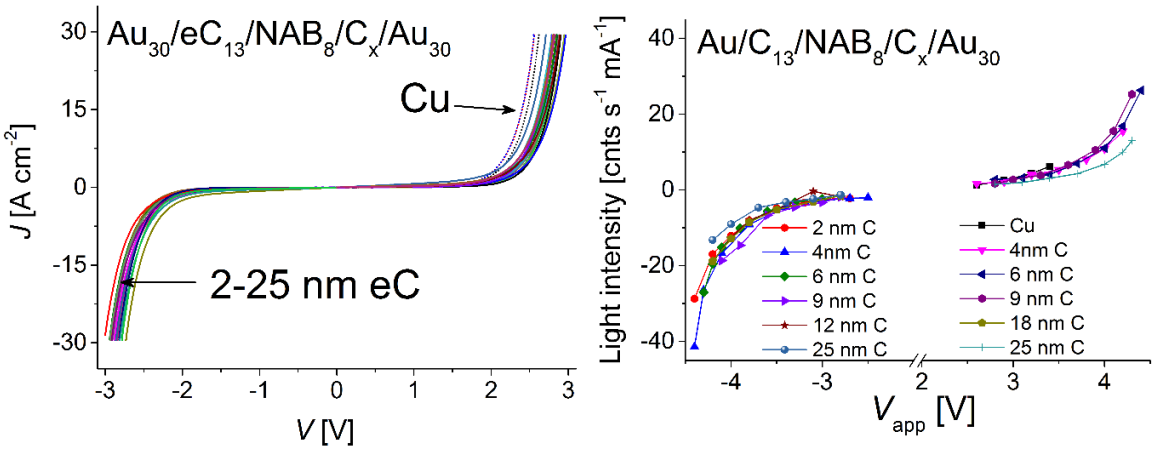


**Figure S9**. Effect of variation of eC thickness from 0 nm (imitated with Cu contact) to 25 nm on *JV* curves (left panel) and intensity of light emission (right panel). All measured *JV* curves overlay closely, confirming similarity of electronic properties for junctions with 2-25 nm of eC. The similarity of the normalized intensity of light emission (cnts/s/mA) and the *JV* curves for both polarities indicates similar light emission mechanisms for both polarities.

## 8. Molecular and contact layer deposition

NDI, NAB, and AQ diazonium salts were synthesized as previously reported by diazotization of the aromatic amine precursor.[3,4] The BTB aromatic amine precursor was obtained from the laboratory of Jean-Christophe Lacroix at the University of Paris, where it was synthesized as described previously.[5] The BTB diazonium ion was prepared in situ according to the procedure described below. The structure of molecular junctions is reported starting from the bottom contact followed by a name of a molecule (Mol) and ending with the top contact which faced the microscope objective, e.g. $Au_{30}/eC_{10}/Mol_x/eC_3/Au_{20}$, with thickness of each layer in nm indicated as a subscript. All of the reported junctions were fabricated with the same substrate on Si/SiOx wafer, $Si/SiOx_{300}/Cr_4/Au_{30}/eC_{10}/$. Unless stated otherwise, light was observed through a top contact of $/eC_3/Au_{20}$, which was approximately 50% transparent to visible light. Fabrication of large area (0.00068 $cm^2$) molecular junctions with the complete structure Si/SiOx/$Cr_4$/$Au_{30}$/eC/Mol/eC/Au consisted of 3 steps: 1) preparation of a bottom contact by evaporation of Cr/Au/eC on a Si/SiOx substrate; 2) grafting of molecular layer; 3) evaporation of the top contact. $Si/SiO_2$ diced wafer chips (1.85×1.3 cm) with 320-340 nm silicon oxide layer were cleaned by sonication in acetone, isopropanol and water for 20 min in each solvent and dried with a stream of $N_2$ before loading into the electron beam deposition system.
(1) The bottom contact was deposited by consecutive evaporation of 3 nm Cr (99.998%, Kurt J. Lesker) at 0.2 Å/s rate; 30 nm of Au (99.99%, MRCS Canada) at 0.2 Å/s rate; and 10 nm C from high purity graphite (SPI supplies, 2spi.com) at a rate of 0.2 Å/s in a Johnsen Ultravac e-beam evaporator at a base pressure $<2x10^{-6}$ Torr. Four vertical lines (250 µm wide) on a chip were prepared through a shadow mask and to serve as the substrate for step 2 (electrochemical grafting of the molecular layer). The RMS roughness of the bottom contact was 0.6±0.1 nm, as determined by AFM.

(2) Preparation of multilayer molecular films was conducted using the electrochemical reduction of diazonium salts of several molecules: nitroazobenzene (NAB), azobenzene (AB), and a phenyl-naphthalene di-imide derivative (NDI).[4] Grafting was performed using a CH Instruments potentiostat with a three electrode cell. Si/SiOx/Cr/Au/eC electrodes prepared in step (1) were used as a working electrode, with a Pt wire auxiliary and $Ag/Ag^{+}$ reference electrodes. The solution for grafting consisted of 1mM diazonium salt precursor (NAB, AB, NDI) with 0.1 M tetrabutylammonium tetrafluoroborate supporting electrolyte in acetonitrile. The solution was purged with high-purity Ar gas for 20 min prior to electrochemical scanning. Freshly evaporated bottom electrodes were used immediately after removal from the deposition system for functionalization. Table S1 contains experimental conditions used to grow molecular films. After grafting, substrates were carefully rinsed with acetonitrile, dried with a stream of $N_2$, and introduced into the electron beam system for evaporation of the top contact, step (3). Preparation of films of BTB was done as described previously[5] under experimental conditions listed in table S1.

(3) $C_3/Au_{20}$ evaporated at 0.2 Å/s rate at a pressure $<2\times10^{-6}$ mbar was deposited horizontally across the substrate lines through a shadow mask to serve as the top contact. Completed junctions were removed from the vacuum chamber and stored in air for 12 h before light emission measurements.

Molecular layer thicknesses were determined using atomic force microscopy (AFM) with a DI-NANOMAN 3100. SPM probes from MikroMasch with a resonance frequency of ~325 kHz and spring constant of ~40 N/m were used for the measurements. A 1×1 um area of the sample SiOx/Cr/Au/eC/NAB immediately adjacent to the junction used for light emission was "scratched" in a contact AFM mode to create a trench.[7] A set point for "scratching" was used according to the thickness (expected from electrochemical grafting conditions) in a range 0.4-0.9 V, where 0.4 V was used for thinner junctions (3-5 nm), progressively increasing to 0.9 V for the thickest 60 nm junctions. A subsequent 5×5 um image collected in tapping mode was analyzed to determine molecular layer thickness by using Gaussian fits to height histograms of the image with the mean difference between height of molecular surface and underlying substrate surface, with a typical thickness standard deviation of ±0.5 nm.[6,8] Thicknesses and standard deviations are listed for all junctions used for light emission in **Table S1**.

**Table S1.** Electrochemical conditions for molecular layer deposition

| Molecule | Thickness [nm] | Starting potential [V vs. $Ag/Ag^+$] | Maximum negative potential [V] | Scan rate [$V\ s^{-1}$] | Number of cycles |
|---|---|---|---|---|---|
| NAB | 3.3 ± 0.3 | 0.4 | -0.43 | 0.2 | 3 |
| | 5.4 ± 0.4 | 0.4 | -0.45 | 0.2 | 4 |
| | 6.1 ± 0.4 | 0.4 | -0.5 | 0.2 | 5 |
| | 8.0 ± 0.5 | 0.4 | -0.75 | 0.2 | 8 |
| | 10.1 ± 0.5 | 0.4 | -0.9 | 0.2 | 8 |
| | 16.2 ± 0.5 | 0.4 | -1.0 | 0.2 | 8 |
| | 19.3 ± 0.6 | 0.4 | -1.05 | 0.2 | 8 |
| | 26.7 ± 0.7 | 0.4 | -1.15 | 0.2 | 8 |
| | 27 ± 0.7 | 0.4 | -1.1 | 0.2 | 8 |
| | 32 ± 1 | 0.4 | -1.25 | 0.2 | 8 |
| | 38 ± 1 | 0.4 | -1.15 | 0.2 | 8 |
| | 40 ± 1 | 0.4 | -1.2 | 0.2 | 8 |
| | 46 ± 2 | 0.4 | -1.25 | 0.2 | 8 |
| | 59 ± 2 | 0.4 | -1.3 | 0.2 | 8 |
| BTB | 7.0 ± 0.3 | 0.4 | -0.4 | 0.1 | 2 |
| | 10.2 ± 0.4 | 0.4 | -0.4 | 0.1 | 4 |
| | 13.4 ± 0.5 | 0.4 | -0.6 | 0.1 | 4 |
| | 21.0 ± 0.6 | 0.4 | -0.6 | 0.1 | 10 |
| | 25.8 ± 0.7 | 0.4 | -0.65 | 0.1 | 10 |
| | 27 ± 0.7 | 0.4 | -0.7 | 0.1 | 10 |
| NDI | 7.9 ± 0.5 | 0.3 | -0.6 | 0.05 | 10 |
| | 9.4 ± 0.5 | 0.3 | -0.6 | 0.05 | 10 |
| | 17.4 ± 0.5 | 0.3 | -0.65 | 0.05 | 10 |
| | 25.5 ± 1 | 0.3 | -0.7 | 0.05 | 10 |
| | 41.5 ± 2 | 0.3 | -0.75 | 0.05 | 10 |
| | 62 ± 2 | 0.3 | -0.8 | 0.05 | 10 |
| AQ | 4.5 ± 0.3 | 0.4 | -0.5 | 0.04 | 8 |
| | 5.2 ± 0.3 | 0.4 | -0.6 | 0.04 | 8 |
| | 9.6 ± 0.4 | 0.4 | -0.7 | 0.04 | 8 |
| | 18.0 ± 0.5 | 0.4 | -0.8 | 0.04 | 8 |
| | 26.0 ± 0.6 | 0.4 | -0.9 | 0.04 | 8 |

## 9. Additional $h\nu_{co}$ values for four molecules and a range of thicknesses

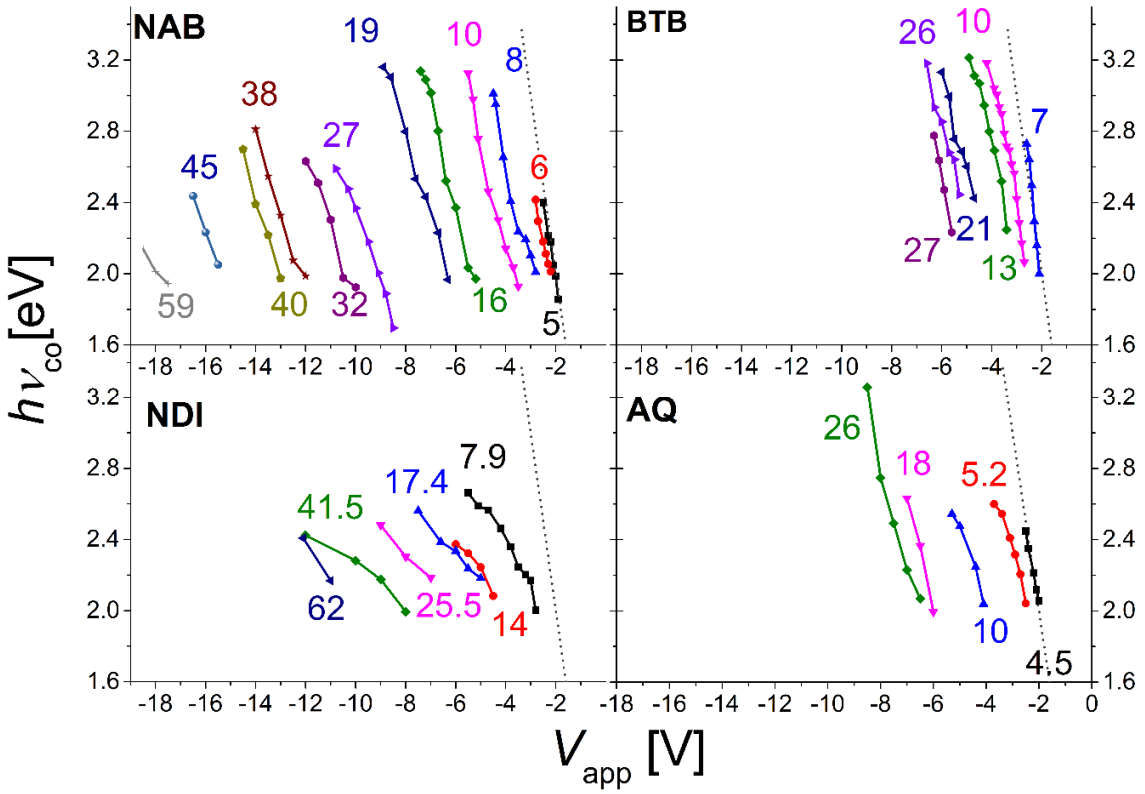


**Figure S1.** Overview of cut-off values for the complete set of thicknesses for each molecule NAB, BTB, AQ, NDI. The elastic line ($h\nu_{co}=eV_{app}$) was added to guide the eye. Junction thickness in nm is indicated next to each line. $V_{app}$ is reported as the DC bias at the bottom electrode with respect to the top electrode in four wire method. Top contact in each case was $eC_3/Au_{20}$.

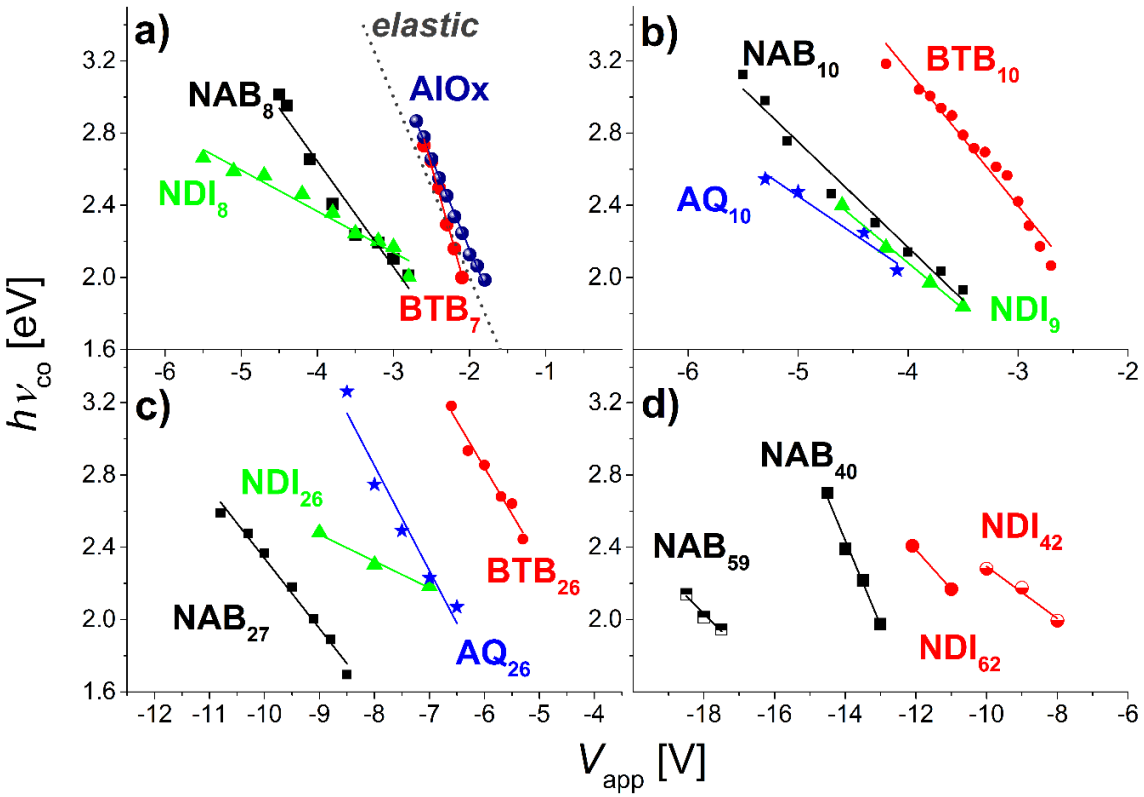


**Figure S10.** Comparison of maximum photon energy as a function of applied bias for a range of thickness 7-62 nm of NAB, BTB, AQ and NDI. $h\nu_{co}$ were determined on raw, uncorrected spectra. a) 7-8 nm, b) 9-10 nm, c) 26-27 nm, d) 40-62 nm. In a) elastic line ($h\nu_{co}=eV_{app}$) and cut-off values for AlOx were added for comparison.

**References for Supporting Information:**


[1] O. Ivashenko, A. J. Bergren, R. L. McCreery, *J. Am. Chem. Soc.* **2016**, *138*, 722.

[2] J. R. Taylor, *An Introduction to Error Analysis: The Study of Uncertainties in Physical Measurements*, University Science Books, Sausalito, California 1997.

[3] A. O. Solak, L. R. Eichorst, W. J. Clark, R. L. McCreery, *Anal. Chem.* **2003**, *75*, 296; Y.-C. Liu, R. L. McCreery, *J. Am. Chem. Soc.* **1995**, *117*, 11254.

[4] J. A. Fereiro, M. Kondratenko, A. J. Bergren, R. L. McCreery, *J. Am. Chem. Soc. 2015, 137*, 1296.

[5] C. Fave, Y. Leroux, G. Trippe, H. Randriamahazaka, V. Noel, J.-C. Lacroix, *J. Am. Chem. Soc.* **2007**, *129*, 1890.

[6] H. Yan, A. J. Bergren, R. McCreery, M. L. Della Rocca, P. Martin, P. Lafarge, J. C. Lacroix, *Proc. Natl. Acad. Sci.* **2013**, *110*, 5326.

[7] F. Anariba, S. H. DuVall, R. L. McCreery, *Anal. Chem.* **2003**, *75*, 3837.

[8] S. Y. Sayed, J. A. Fereiro, H. Yan, R. L. McCreery, A. J. Bergren, *Proc. Natl. Acad. Sci.* **2012**, *109*, 11498.